NOVA SCHOOL OF SCIENCE & TECHNOLOGY

DEPARTMENT OF CHEMISTRY

CAROLINE TUREK

BSc in Biology applied to health

# Specific detection of nucleic acids and/or other bioanalytes for point-of-care diagnosis of tropical diseases

MASTER IN BIOTECHNOLOGY

NOVA University Lisbon
September, 2023

DEPARTMENT OF CHEMISTRY

# Specific detection of nucleic acids and/or bioanalytes for point-of-care diagnosis of tropical diseases

**CAROLINE TUREK**

BSc in Biology applied to health

**Adviser:** André do Rosário Magalhães
*Development Director, biosurfit*

**Co-adviser:** Catarina Caneira
*Senior Research & Development Engineer, biosurfit*

**Examination Committee:**

**Chair:** Dr. Ana Rita Cruz Duarte,
Associate Professor with habilitation, FCT-NOVA

**Rapporteurs:** Dr. Pedro Miguel Ribeiro Viana Baptista,
Full Professor, FCT-NOVA

**Adviser:** Dr. Catarina Raquel Fernandes Caneira,
Senior Research & Development Engineer, biosurfit

MASTER IN BIOTECHNOLOGY
NOVA University Lisbon
September, 2023

**Specific detection of nucleic acids and/or other bioanalytes for point-of-care diagnosis of tropical diseases**

# ACKNOWLEDGEMENTS

This thesis wouldn’t be the same without all the people who were by my side during this year that concludes the end of the master’s degree.

I would like to thank Maria João Costa and André Magalhães for welcoming me to the company biosurfit and the R&D department, for all the patience with those weekly Friday meetings. Thank you also to everyone in the company biosurfit who guided me in my first steps in the corporate world, especially the people from the HR, logistics and production departments who were always there to help when needed (even when the language barrier was sometimes present with my bad Portuguese).

Thank you to Prof. Maria Ascensão Reis from FCT NOVA for taking the time to find me this thesis work, this was the starting point of this whole project for me.

Special thanks to Catarina Caneira for all the work and time you’ve put into this project to help and guide me, for the motivation, for teaching everything you could during this year, always being there through the countless PCRs and RPAs, coaching me before every weekly meeting. I definitely have learned so much from you.

A massive thank you to all my colleagues from the R&D department, each person contributed in their own way to this project, always there to give advice and an external point of view on the project and giving me a bit of their experience.

To Clisiane Santos and Marta Marques for the friendship during this year, for sharing your life experiences, for the constant support, for all those endless conversations after lunch with Clisiane and during those Azambuja to Lisboa train rides with Marta, teaching each other words from our own languages.

I would like to acknowledge my friend Carlota Pinheiro without whom I would have not applied for this master's degree in Lisboa, it is crazy how a random conversation in our kitchen in Slovenia in June 2021 ended up with me moving here three months later and living the Portuguese life. I can’t wait to finally have our Portuguese summer together when you’re back from Asia.

To André Piteira, for the great friendship, support and the red velvet cake conversations.

To Sandro Amador, for being such a good friend (also a good representative of the master’s degree), who was always there for extra motivation, especially during this year of the thesis, I know that I can always count on you. Even though this master’s degree is reaching its end, I know that this friendship will still last for years.

To Katia Luz, for being my partner in this master's, always having each other’s back, this random pairing for the REG lab practicals two years ago led to one of the best friendships. Thank you also for your wisdom, you are definitely an example for me. I’m glad that we’ve managed to keep our little pact until now and that it will still be valid for the next years! I’m so glad and proud to see how much we’ve evolved those two past years menina.

To David Reis, for being my colleague from the master’s degree, best friend and boyfriend at the same time. Thank you for always having the right words, making me laugh, and the unconditional support at all times. Estou feliz por termos dado este novo passo juntos e por nos termos conseguido apoiar durante este percurso. Obrigada por tudo.

À mes parents et ma sœur pour le soutien et les encouragements durant cette phase finale de mes études, la motivation dans l’écriture de ce mémoire et pour le nouveau projet qui m’attend le mois prochain, merci.

# ABSTRACT

Dengue (DENV), Chikungunya (CHIKV), and Zika (ZIKV) viruses present similar high-fever symptoms, making them challenging to differentiate and potentially leading to serious complications without early detection and treatment. Point-of-care (POC) diagnoses are crucial, especially in low and middle-income countries where these viruses are prevalent. POC devices enclosing nucleic acid isothermal amplification, are a faster alternative to the gold standard, Polymerase Chain Reaction, simplifying the process, requiring lower and constant temperature, and providing accurate results for early virus detection and proper treatment.

In this study, we developed a rapid DENV detection method using a centrifugal microfluidic cartridge combined with isothermal Recombinase Polymerase Amplification (RPA). Two different optical detection strategies were evaluated: (1) integrated lateral flow assay strip and (2) in bulk fluorescence detection. This work proved the possibility of detection on the microfluidic cartridge by testing different known concentrations of a synthetic dsDNA mix constituted of a complementary primer and a probe specifically designed for the strip, displaying a limit of detection down to 0.54 nM with cartridge sample processing. Furthermore, RPA optimization was conducted for both detection strategies. Successful RPA off-chip amplification and on-chip signal detection of a synthetic cDNA representative of the three prime untranslated region gene was achieved within 35 minutes. Using the lateral flow strip detection, the results displayed a significant difference in mean grey value 39-fold higher for the $10^5$ copies/mL target compared to the negative control. RPA off-chip amplification for in-bulk fluorescence detection on-chip was also achieved within 20 minutes, showing promising results as an alternative method of detection, possibly allowing quantitative analysis. In the future, further optimization is required for full integration of the assay and detection on the disc, and multiplexing could enhance capabilities, enabling simultaneous ZIKV and CHIKV detection.

Overall, the first steps of a future centrifugal POC DENV detection device were successfully achieved.

**Keywords**: Point-of-care; Microfluidic device; isothermal amplification; RPA; 3'UTR gene, Dengue virus

# RESUMO

Os vírus Dengue (DENV), Chikungunya (CHIKV) e Zika (ZIKV) apresentam sintomas semelhantes de febre alta, tornando-os difíceis de diferenciar e potencialmente levando a complicações graves sem detecção e tratamento precoces. Os diagnósticos point-of-care (POC) são cruciais, especialmente em países de baixa e média renda onde esses vírus são predominantes. Os dispositivos POC que incluem amplificação isotérmica de ácido nucleico são uma alternativa mais rápida ao "gold standard", "Polymerase Chain Reaction", simplificando o processo, exigindo temperatura mais baixa e constante e fornecendo resultados precisos para detecção precoce de vírus e tratamento adequado.

Neste estudo, foi desenvolvido um método rápido de teteção do vírus da dengue (DENV) usando um cartucho microfluídico centrífugo, e "Recombinase Polymerase Amplification" (RPA). Duas estratégias diferentes de deteção foram testadas: (1) uma tira de ensaio de fluxo lateral integrada e (2) deteção de fluorescência em "bulk". Este estudo demonstrou a capacidade do cartucho microfluídico de detetar uma mistura sintética com um limite de deteção tão baixo quanto 0.54 nM. Posteriormente, procedemos a otimização do RPA, para ambas as estratégias de deteção, no qual obtivemos uma amplificação e deteção em apenas 35 minutos. Usando a detecção de faixa de fluxo lateral, os resultados exibiram uma diferença significativa no "grey mean value" 39 vezes superior para o alvo de $10^5$ cópias/mL em comparação com o controlo negativo. A amplificação RPA fora do chip para detecção de fluorescência em massa no chip foi alcançada em 20 minutos, mostrando resultados promissores, possivelmente permitindo uma análise quantitativa. Como trabalho futuro, será necessária uma otimização adicional para a integração total do ensaio e da detecção no disco, e a multiplexação poderá aprimorar os recursos, permitindo a detecção simultânea dos vírus ZIKV e CHIKV.

No geral, os primeiros passos de um futuro dispositivo centrífugo de detecção POC DENV foram alcançados com sucesso.

**Palavras-chave**: POC; cartucho microfluídico; amplificação isotérmica; RPA; Gene 3'UTR, vírus da dengue

# TABLE OF CONTENTS

# LIST OF FIGURES

# LIST OF TABLES

# LIST OF EQUATIONS

# LIST OF ABBREVIATIONS AND SYMBOLS

**3'UTR** – Three prime untranslated region

**5'UTR** – Five prime untranslated region

**Ab** – Antibody

**Ag** – Antigen

**AuNP** – Gold Nanoparticles

**BHQ** – Black Hole Quencher

**bOG** – β-octyl glucoside molecule

**bp** – Base pair

**cDNA** – Complementary Deoxyribonucleic acid

**CHIKV** – Chikungunya virus

**CNP** – Carbon Nanoparticles

**CRISPR** – Clustered regularly interspaced short palindromic repeats

**Ct** – Cycle threshold

**DENV** – Dengue virus

**DNA** – Deoxyribonucleic acid

**dNTP** – Deoxynucleotide triphosphate

**ds** – Double-stranded

**ELISA** – Enzyme-linked immunosorbent assay

**exo** – Exonuclease

**HDA** – Helicase-dependent amplification

**HPLC** – High-performance liquid chromatography

**IDT** – Integrated DNA technologies

**IgG** – Immunoglobulin G

**IgM** – Immunoglobulin M

**IHMT** – Instituto de Higiene e Medicina Tropical

**iiPCR** – Insulated Isothermal PCR

**IPATIMUP** – Instituto de Patologia e Imunologia Molecular da Universidade do Porto

**kb** – Kilobase

**LAMP** – Loop-mediated isothermal amplification

**LFA** – Lateral Flow Assay

**LoD** – Limit of detection

**MDG** – Millennium Development Goal

**NASBA** – Nucleic acid sequence-based amplification

**Nfo** – Endonuclease IV

**NS1** – Nonstructural protein 1

**NS5** – Nonstructural protein 5

**nt** – Nucleotide

**NTC** – Non-template Control

**NTD** – Neglected Tropical Diseases

**PBS** – Phosphate-buffered saline

**PCR** – Polymerase chain reaction

**PLOS** – Public Library of Science

**POC** – Point-of-care

**qPCR** – Quantitative Polymerase chain reaction

**RCA** – Rolling circle amplification

**RNA** – Ribonucleic acid

**RPA** – Recombinase polymerase amplification

**RT** – Reverse transcriptase

**SDA** – Strand Displacement Amplification

**ss** – Single-stranded

**TBS** – Tris-buffered saline

**TBST** – Tris-buffered saline with Tween 20

**THF** – Tetrahydrofuran

**Tm** – Melting temperature

**WHO** – World Health Organization

**YFV** – Yellow fever virus

**ZIKV** – Zika virus

# 1.INTRODUCTION

## 1.1 Tropical diseases

During the last decades, a high incidence of tropical diseases has been observed over the world [1]. The term tropical disease is used for all diseases that occur mainly in the tropics, which covers the regions between the Tropic of Cancer and the Tropic of Capricorn [2]. In the early 2000s, as those diseases didn't receive the same attention as other ones, the term Neglected Tropical Diseases (NTD) appeared in the Millennium Development Goal (MDG) 6 of the United Nations. The list has been expanded multiple times over the years by PLOS Medicine, then the WHO, and more recently by Public Library of Science (PLOS) Neglected Tropical Diseases [3]. The creation of this term, as well as different goals to tackle this issue, has been beneficial since the number of cases worldwide dropped from 2.19 billion in 2010 to 1.73 billion in 2020 according to the WHO. However, the COVID-19 pandemic disrupted the NTD services being one of the health services most affected by the pandemic in 2020. That is why the WHO has a new road map for NTDs (2021-2030) with new actions to reduce the prevalence of those diseases [4]. One way to reduce the prevalence is by performing timely diagnostics to decrease the risk of disease transmission in the community and allow for correct identification and treatment. The development of point-of-care testing (POC) has given us new tools to improve health surveillance and management, especially in underdeveloped areas and help in the fight against NTDs.

## 1.2 Arboviruses

The NTDs list includes Arboviral infections (arthropod-borne viruses) that are spread by arthropod vectors that can be mosquitoes, ticks, and sand flies through bites. There are more than 500 different types of arboviruses, but only a small number can cause human diseases [5]. Arboviruses are mostly characterized by an RNA genome (except with dsDNA for the case of African Swine Fever Virus) [2].

Among those, Dengue virus (DENV), Chikungunya virus (CHIKV), Zika virus (ZIKV) and Yellow fever virus (YFV) can be transmitted by infected female mosquitoes, which gave those viruses the name of *Aedes*-borne viruses. Moreover, they do not only touch the tropics anymore since cases have been reported in Europe this past decade, with the first Chikungunya cases reported in Italy in 2007 and the first Dengue cases reported in France and Croatia in 2010. That expansion of tropical diseases is explained by the surge of air travel worldwide for tourism, work or migration purposes [6]. The main vector of those three arboviruses is the mosquito *Aedes aegypti* (also called yellow fever mosquito) and to a lesser extent *Aedes Albopictus* (Asian tiger). The mosquitos become infected after feeding on a DENV-infected person during its five-day period of viraemia, a period in which the blood contains high levels of the virus. Unlike humans, once a mosquito gets infected, it stays infected until the rest of its

life. The virus reaches the intestinal tract of the mosquito where it incubates for approximately 10 days; sometimes even less depending on the temperature; and then joins the salivary glands, which explains why mosquito bites become infectious.

To this day, no specific treatment exists to this day for *Aedes*-borne viruses, only symptomatic treatments that are being reviewed in **Table 1** [7].

**Table 1: Aedes-borne arboviruses characteristics**, adapted from [7]

| Virus | Type | Symptoms | Supportive treatment |
|---|---|---|---|
| **Dengue** | Flavivirus | Sudden high-grade fever, Headache, Eye & muscle pain, Arthralgia | DENV vaccine & drug administration |
| **Zika** | Flavivirus | Fever, Headache, Conjunctivitis, Joint pain, Microcephaly | Fluid intake & drug administration (Acetaminophen) |
| **Chikungunya** | Flavivirus (*Togaviridae)* | High fever, Conjunctivitis, Joint pain, Arthritis | Rest, fluid intake & drug administration (Acetaminophen) |
| **Yellow Fever** | Flavivirus | Fever, Headache, Joint pain, Nausea | YFV vaccine and drug administration (Ribavirin) |

## 1.3 Flavivirus

Flavivirus is characterized by ssRNA-enveloped virus that is capable of generating high mortality rates. Currently, Dengue is one of the most prevalent viruses of the family but Zika has had recent outbreaks over the past few years [8], [9].

This type of virus can be asymptomatic, or evolve into an important illness such as haemorrhagic fever, meningoencephalitis, and neurological complications and no anti-flavivirus agent is currently being

commercialized. That is why an early and accurate diagnosis of flavivirus infections is important for clinical care, and for the treatment to be administered to patients before the infection exacerbates.

### 1.3.1 Dengue

Today, half of the world's population is at risk of Dengue [10], with Brazil, Vietnam, and the Philippines being the most affected countries as seen in **Figure 1**. In the year 2022, between January and August, 2 597 067 cases and 2 065 deaths have been reported in the world [11]. It is the most widespread flavivirus and deadliest of the *Aedes*-borne viruses [12]. Alongside the transmission by mosquitoes, some cases of human-human transmission via blood transfusion have been reported [13]. It is estimated that approximately 2/5 of the world's population is at risk of developing an infection due to that virus [14]. A myriad of cases are asymptomatic or only cause mild illness with symptoms similar to the flu, and the true number of cases might be considerably higher. The common symptoms are high fever, headaches, vomiting, myalgia, and joint pain. After this phase of symptoms, the patient usually recovers by itself, except in some cases where it evolves into Dengue Haemorrhagic Fever that can cause circulatory failure as well as death.

DENV is caused by an RNA virus of the Flaviviridae family and has four different serotypes: DENV-1, DENV-2, DENV-3 et DENV-4 and it is possible to be infected by every single one of them, which means that it is possible to be infected by DENV-1 and then have immunity against this serotype but still be able to be infected by each of the other three serotypes. Moreover, subsequent infections increase the risk of developing severe dengue, also called haemorrhagic shock syndrome [15], and it can cause death in some severe cases [10]. There is currently no vaccine available for the general population, only a recently introduced vaccine for seropositive individuals in a specific age range, due to the differential efficiency [16]. The best chance to avoid the severe type is an early and accurate detection of the disease.

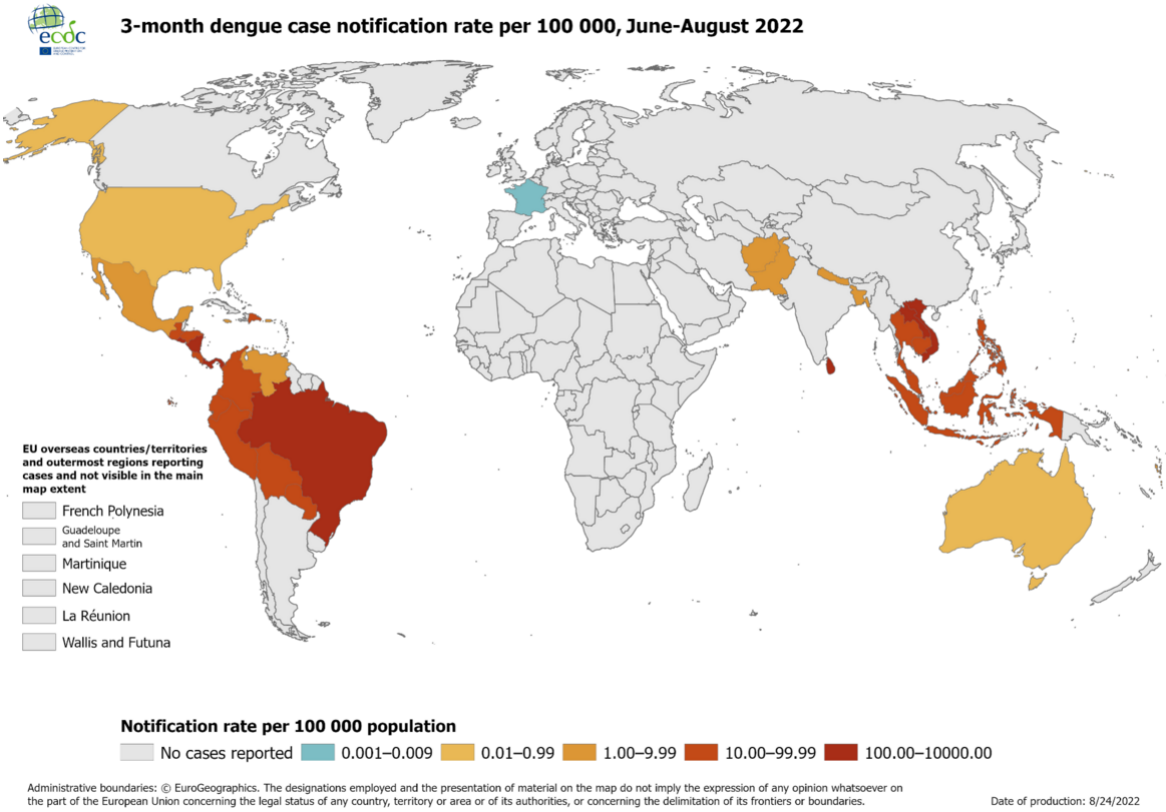


**Figure 1: Cases of DENV worldwide between Jun-Aug 2022** [17]

DENV is spherical and has a 40-60 nm size. It contains the viral RNA and C proteins in the nucleocapsid, surrounded by a lipid bilayer (envelope) [18] that contains the E and M proteins embedded in it (**Figure 2**). It has a positive-sense ssRNA and a complete genome of 11 kb, that encodes for 3 structural proteins: E (Envelope), C (Capsid), and M (Membrane) and seven non-structural proteins (NS): NS1, NS2A, NS2B, NS3, NS4A, NS4B, and NS5 [19] as shown in **Figure 2**.

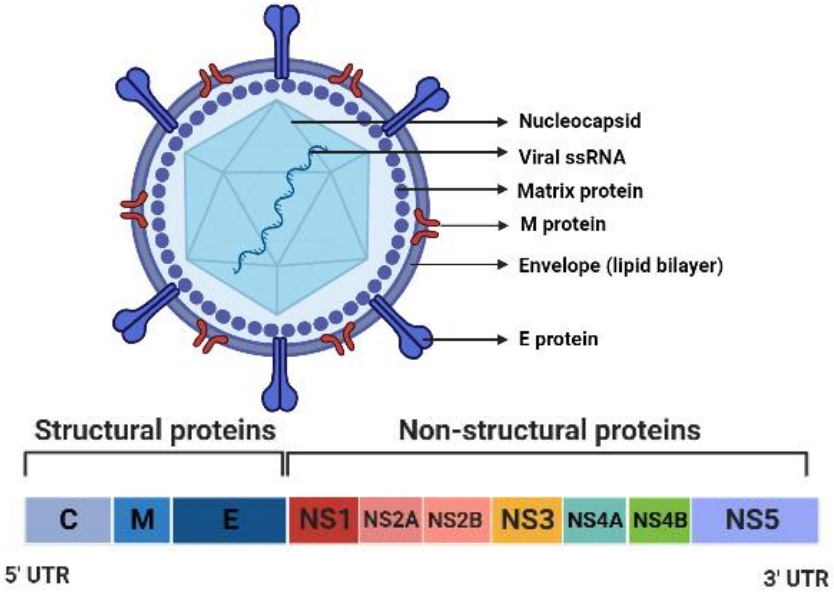


**Figure 2: DENV structure, designed on** [20]

The DENV has a characteristic envelope of flaviviruses, that contains a star-shaped element (in blue in **Figure 3**). It is a part of the dimer formed by the protein E present on the envelope [21].

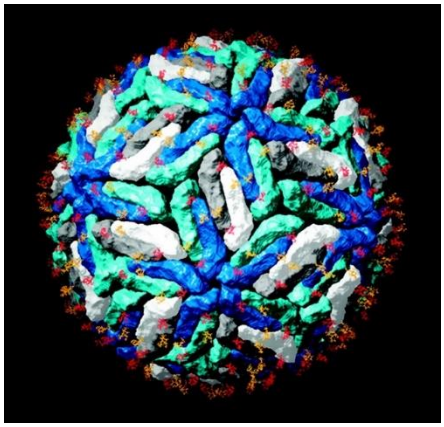

**Figure 3: Dengue virus envelope glycoprotein structure reconstituted with Ribbons after observation by cryogenic electron microscopy** [21]

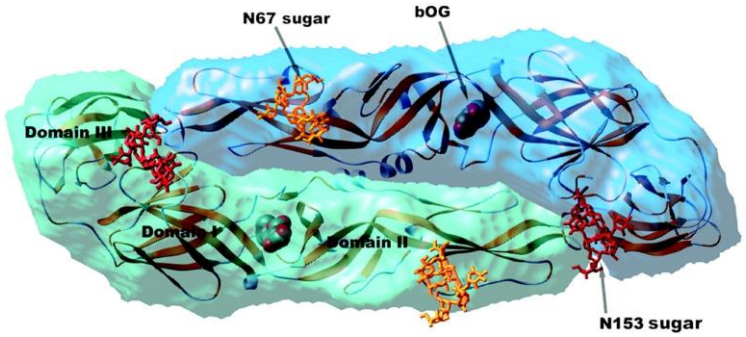


**Figure 4: Representation of the two dimers constituting the E protein of the DENV** (same colour coding as in Fig. 3) [21]

Indeed, as displayed in **Figure 4**, protein E is made of two dimers, one constituted of three domains while the other one is made of sugars and of a β-octyl glucoside molecule (bOG). The second one lies in a pocket between domains I and II. That region is known to have lots of mutations which are likely to trigger conformational changes that lead to membrane fusion [21] with the membrane of the target cell, which results in the infection of the host of the cell [22].

### 1.3.2 Zika

80% of Zika infections are asymptomatic, hence why the virus was first seen as insignificant but it can also show a wide range of symptoms that are similar to Dengue: arthralgia, oedema, mild fever, headaches, conjunctivitis, vertigo, and myalgia [23], [24]. Eventually, it became a global health emergency as Zika has been linked with severe diseases, such as multi-organ failures and neurological diseases such as the Guillain-Barré Syndrome, meningitis, microcephaly, and congenital Central nervous system malformations [25]. Moreover, some cases of secondary nonsexual transmission have been reported, as patients in contact with body fluids such as sweat or tears from highly infected ZIKV patients ended up contracting the virus [24].

### 1.3.3 Chikungunya

Chikungunya virus (CHIKV) has re-emerged recently and also causes similar symptoms to the two previous diseases mentioned aforementioned: fever, severe joint pain, and myalgia. Those symptoms can last for weeks and sometimes even for months. Like the two other diseases, some cases of CHIKV can be severe with the same symptoms as severe arthralgia and neurological symptoms presented before. The severe arthralgia can last for years in some cases which can cause poor mobility in everyday life [26]. Moreover, the impact of the Central nervous system and the hepatitis cases, shows that the disease evolved into a more aggressive and severe form [27]. The name of the disease came after the description of the symptoms by the local Makonde population in Tanzania which translates as “disease that bends up joints” and was first seen as a type of Dengue virus back then [28]. Some cases of CHIKV can also be asymptomatic, even though it is quite rare, from 3 to 28% of the total cases only (varies in function of the outbreaks), but can have an impact on the transmission of the virus, for example in the case of blood donation, where the transfusion of CHIKV infected blood will transmit the virus [29].

## 1.4 Diagnosis of flavivirus infection

With the current outbreak, it is essential to have accurate, specific, and easier detection of a flavivirus infection as early detection allows for better clinical care of the patient, which is relevant since there is no specific antiviral treatment, and allows prevention of the spread of the disease by avoiding contact with humans and mosquitoes when the diagnostic is made.

There are various methods of detection, but the main ones are the detection by antibody serology, NS1 antigen, or flavivirus-specific nucleic acid detection. The confirmation of the diagnosis is crucial as it allows better clinical care, but also reduces the need for expensive investigations [30]. In fact, since 2014 Brazil has been going through waves of epidemics of triple flaviviruses: Dengue is re-emerging, and Zika and Chikungunya emerging. The Brazilian health system has a hard time managing the outbreaks, due to the difficulty of diagnosis (since the symptoms are similar) and lack of a protocol

for patient treatment, which shows even more the emergency of being able to test with reliability and rapidity [31].

However, it has been reported that less than half of the Dengue cases (48.72 %) have been confirmed by laboratory testing in America in 2022 according to WHO [32]. The numbers for flavivirus testing are low in the whole world and tend to decrease in poorer countries as accurate testing is shown to be expensive and time-consuming, as displayed in the report by stating that 100% of Dengue fever have been laboratory-confirmed in North America but for South America the numbers considerably decrease, explaining the low percentage for the South American continent [32]. Also, the different testing methods have different sensitivity and specificity which impacts the accurate number of cases [33].

### 1.4.1 Antibody serology

The antibody serology is the most common method of detection, it consists of measuring the Immunoglobulin G (IgG) or Immunoglobulin M (IgM) antibodies by ELISA (enzyme-linked immunosorbent assay). It is an easy technique to perform but still requires laboratory equipment and trained staff [34], and the sensitivity and specificity can sometimes be lacking for the application required[16]. Since the rise of the IgM levels for a primary infection is not immediate and is progressive, the sensitivity of the test is very low during the first 4 days of the infection, which doesn't allow the use of this method for an immediate accurate diagnostic [35]. The problem is also present for the detection of secondary infection, as the level of IgM is lower (as the response of the immune system is faster and more efficient with lower levels of IgM) so false-negative results happen in >20% of cases; and the values of IgG are higher in those cases, so a ratio between IgM and IgG has to be done to diagnose efficiently those secondary cases that are more severe [16].

But the major issues are that the IgM circulates for 60 days, and IgG circulates throughout life, so the positive result could mean either a current infection or a recent infection, and it would be impossible to distinguish them both. The other main issue is the cross-reactivity between the different flaviviruses. In a study, 42% of patients vaccinated against Yellow Fever were dengue IgM positive, while all of them were negative and healthy prior to vaccination. In summary, the detection of an anti-DENV antibody (Ab) could result in a DENV infection, an infection by another flavivirus, or the result of the vaccination against another flavivirus (which would bias the result of the test in the case of an accurate case of DENV), that is why this type of test would require two samples, taken at different stages of the infection (acute viraemia and during convalescence stage) [36].

### 1.4.2 Non-structural protein 1 (NS1)

NS1 is a conserved glycoprotein produced from infected cells, that is essential for the virus viability as its glycosylation is important for the efficient secretion, virulence, and viral secretions [37]. It can be quantified for the detection of flavivirus infections as it is present during the viraemic phase of the infection and allows rapid detection.

However, the two main downsides are that for secondary infections, the NS1 window of detection is smaller and has a smaller sensitivity to the interaction Ab-Ag (antigen) with IgG [38], which is once again a problem as those infections are more severe. In addition, the sensitivity varies widely depending on the serotype of the virus [39].

Overall, this type of test can be interesting coupled with the antibody serology mentioned before, as those two types of detection can be complementary.

### 1.4.3 3'UTR gene

In flaviviruses, Untranslated regions (UTR) consist of many RNA structural elements involved in the replication. The 5'UTR region is a short sequence of about 100 nucleotides (nt), that contains an RNA synthesis promoter and a cyclisation sequence that mediates long-range RNA-RNA interactions [40]. The other UTR region is the 3'UTR region which has the advantage of having a similar general organization in all flaviviruses. It has a longer sequence than the 5'UTR (about 450 nt), and its key feature includes high conservation of sequence repeats and duplicated RNA structures through the evolution, which are both essential for replication. Moreover, it possesses secondary structures that allow for more stability in the genome and prevent its degradation [41], [42].

In the dengue virus, the two structures essential for replication in the 3'UTR gene are a 3'end that folds into a stem-loop that is highly conserved and forms a 3'SL. Upstream this 3'SL, a cyclisation sequence can be found that is complementary to another sequence in the 5' end and allows 5'-3'RNA-RNA interactions that are important in the replication process of the Dengue virus [43].

### 1.4.4 Nucleic Acid Amplification Tests

#### *1.4.4.1 PCR (Polymerase Chain Reaction)*

The PCR is the “gold standard” for nucleic acid testing as it can detect viral RNA with high sensitivity and specificity [44].

It allows the amplification of a specific DNA fragment, also called target sequence, with only traces of DNA needed to perform the PCR which will give enough copies of DNA to be detected by conventional methods. It requires template DNA, primers, free deoxynucleotides (such as Deoxynucleotide triphosphate (dNTP)), and a DNA polymerase [45] called Taq. Taq comes from Thermus Aquaticus, a thermophile. It is an organism that can grow at very high temperatures (>100°C) which means that it won’t be damaged during the different cycles at high temperatures [46]. The DNA polymerase will link all the nucleotides together to form the product of the amplification of PCR, while the primers will help specify exactly which part of the DNA sequence needs to be amplified, as they are small sequences complementary to the target DNA sequence [45], [47]. In addition, the DNA polymerase can only start adding nucleotides to a 3’-OH group, present in the primer. This is why primer design is key in the design of the experiment, as the primers will determine the outcome of the experiment [46]. The amplification is then carried on a thermal cycler, as PCR consists of a few steps at different temperatures. PCR can be used for diagnostic purposes, as it has widely been used during the pandemic of SARS-CoV-2. As viruses are present in small quantities in a sample, the amplification of the nucleic acid of a particular virus will allow the detection of it with good specificity and sensitivity [48].

PCR recommendations for experimental design include melting temperatures between 55-70°C, with a 5°C difference maximum between two primers, GC content between 40-60%, a C or G nucleotide at the 3’end, a length of 15-30 bp and no more than 3 G or C nucleotides in a row at the 3’end [49].

The first step is denaturation, where the DNA is melted to separate the strands from each other. To do so, the temperature must rise above the melting temperature of the DNA strands (usually 95°C), which will break the hydrogen bonds between the complementary bases and will give single-stranded DNAs (ssDNAs) instead of the initial dsDNA. Secondly, the annealing step allows the primers to bind to their complementary sequence of the target DNA, which takes place at a lower temperature than the previous step. To finish, the extension step extends the primer amplified strand using the DNA polymerase by adding nucleotides to the strand end. This step is carried at a higher temperature, usually 72°C as it is the polymerase’s optimal temperature. Those three steps are part of one cycle that allows the doubling of the quantity of DNA from cycle to cycle, as shown in **Figure 5**. PCR usually consists of many cycles, between 20-50 cycles, to reach billions of copies of DNA [45], [47]. After that, the reaction usually produces a plateau phase as the activity of the Taq polymerase starts to decrease [46].

Complementary analysis is needed to verify that the amplification occurred, and, in the end, we obtained the product of amplification expected. The product of amplification is run on an agarose gel and stained with a dye that will intercalate between the two strands, allowing detection. More specifically, the agarose gel is submerged in the electrophoresis buffer containing salts. Then the product of

amplification is introduced to the wells and an electric current will pass through the gel. Each end has an electrode (positive on one side and negative on the other) and since the DNA is negatively charged, it will migrate towards the positively charged side. The smaller fragments will reach the other side faster than the bigger ones, which will allow the determination of the different sizes of each fragment. The agarose gel electrophoresis will in this way separate the DNA product by amplicon size, and different bands will appear in the gel. The fluorescent intercalating dye, when exposed to UV light, allows us to clearly see the DNA. The most common dyes used are SYBR Green, GelRed, and Ethidium Bromide. By having a DNA scale in one of the agarose gel lanes, the size of the DNA products will be known, by comparison with the reference bands [45], [47].

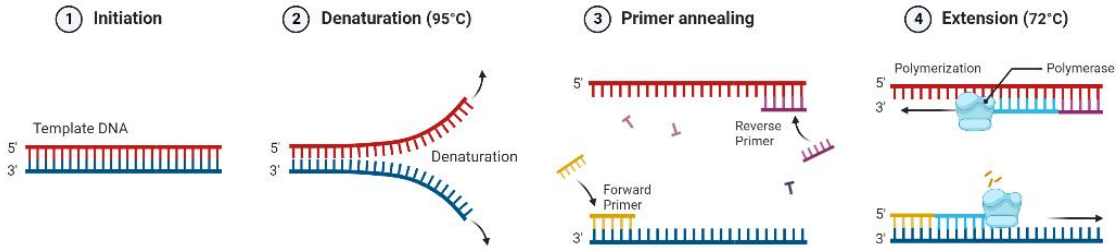


**Figure 5: Mechanism of Polymerase Chain Reaction, where steps of Initiation (1), denaturation (2), primer annealing (3), and Extension (4), are schematized**, adapted from [20].

### *1.4.4.2 qPCR (quantitative PCR)*

An alternative nucleic acid amplification technique is the quantitative real-time PCR (qPCR). To be able to detect and quantify the product [50], it is either possible to use fluorescent dyes or a probe specific to the DNA sequence that is fluorescently labelled and possesses a quencher. The probe will hybridize with the cDNA and allow the real-time monitoring of the levels of fluorescence throughout the amplification, which will be exponential if the amplification is correctly carried on, as the level of fluorescence is linked to the number of copies of the target gene (**Figure 6**). The fluorescence is detected when the fluorescent dye is cleaved from the quencher. The whole method relies on the 5'→3' exonuclease activity of the Taq DNA polymerase. That method makes unnecessary the gel electrophoresis step since only the qPCR is required for fluorescence detection [45]. To choose between the fluorescent intercalating dye or the probe (which is a fluorescently labelled DNA oligonucleotide), a few elements must be taken into consideration: the cost, as the probe is more expensive, but also the specificity required. Indeed, the probe is more specific as the fluorescence only occurs when the binding between the primers and the probe is correct and they can only bind at the exact target sequence desired. Intercalating dyes are non-specific and there is a risk of an amplification of the wrong target which would give a fluorescent signal [47].

Carboxyfluorescein (FAM) is a 5'end popular reporter dye, while Carboxytetramethylrhodamine (TAMRA) is a 3'end common quencher. Recently, as an alternative to TAMRA, Black Hole Quencher (BHQ) has been widely used to reduce the high background noise in fluorescent signals associated with

TAMRA. BHQ doesn't emit light since it re-remits its energy in the form of heat, allowing it to decrease fluorescence noise in an effective manner [51]. Moreover, BHQ uses modified C and T nucleotides which allows for more probe-target duplex stability, and therefore it is possible to design shorter nucleotides. The use of shorter nucleotides has the advantage of being cheaper when compared with longer ones [52].

When the initial material to detect is ribonucleic acid (RNA), instead of DNA, a starting step of reverse transcription (RT) is performed to synthesize cDNA from the RNA template. After that initial step, the amplification proceeds like it was explained before [53].

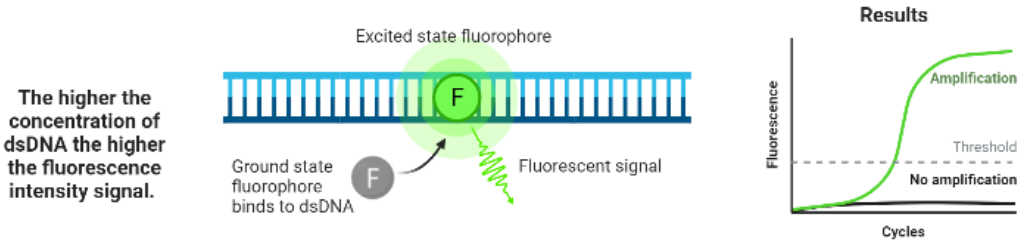


**Figure 6: Principle of qPCR where a fluorescence dye intercalates in the dsDNA and emits fluorescence**. The ground state fluorophore will bind to the dsDNA and when reaches the excited state, will emit a fluorescent signal that will allow the quantification of the concentration of dsDNA it is bound to. The fluorescence will be detected from cycle to cycle given the amplification plot illustrated on the right, adapted from [20].

PCR is the standard amplification method and despite the advantages its main downsides are that any contamination will have an impact on the results because of its high sensitivity [54], the slightly long time of amplification (~1h30min, without sample preparation) and is very expensive due to its thermal cycler (that has cost values in the order of 10000€ or above [55]) and also consume high levels of energy. Over the past few years, techniques for qPCR have been developed and improved, which are faster to perform and have less chances of contamination while having similar rates of specificity and sensitivity, like one-step qRT-PCR kits that allow to limit the risks of carryover contaminations [56].

To quantify the results of a qPCR, a calibration curve is used that correlates the cycle threshold (Ct) to known concentrations (quantified genetic material) of the product of amplification under analysis. It represents the number of cycles required for the fluorescence levels to cross a threshold, which is the value where it exceeds the background levels. Those values are inversely proportional to the amount of nucleic acid in the sample. Ct values ≤ 29 are strong positives, between 30-37 are considered positives, and below are weak reactions that could be the result of contamination [57]. A very effective way to quantify this data obtained is to evaluate the qPCR efficiency by making a calibration curve of the target and using the Ct values obtained. The slope of the curve obtained allows us to calculate the efficiency. For example, for a quantity of nucleic acid that is doubled during one cycle of the amplification, the qPCR efficiency will correspond to 100%, which implies that the higher is efficiency, the better the amplification. However, an efficiency exceeding 100% will be the result of polymerase inhibition, as the quantity of template DNA added would increase but the Ct value wouldn't be lower, which would result in lowering the slope and giving an efficiency over 100%. An efficiency below 100% would imply further optimization

of the assay as it could be due to an inadequate melting temperature (Tm), or primer design or the formation of a dimer. A good, expected efficiency would be in the range of 90-110% [58].

### *1.4.4.3 Isothermal amplification*

The requirements of the temperature cycle in PCR, and the consequent need for a thermocycler, increase the costs of the assays and restrict the process to a laboratory infrastructure. On the other hand, an isothermal amplification occurs at a constant temperature, decreasing the temperature requirements, and a simple heating block can be used. Furthermore, it is easier and cheaper to integrate on-chip a temperature control set to a unique temperature than the integration of temperature control involving temperature cycles. That is why, isothermal amplification methods have been widely developed in the past decades, with a special focus on point-of-care (POC) diagnosis [44]. Some of the most popular isothermal amplification techniques are NASBA (Nucleic Acid Sequence Based Amplification), SDA (Strand Displacement Amplification), RCA (Rolling Circle Amplification), LAMP (Loop-Mediated Isothermal Amplification) and RPA (Recombinase Polymerase Amplification) [59].

**Table 2: Comparison of the main properties of the main isothermal amplification techniques**, adapted from [44], [59]

| | **NASBA** | **RCA** | **RPA** | **SDA** | **LAMP** |
|---|---|---|---|---|---|
| **Target** | RNA | DNA/RNA | DNA | DNA | DNA |
| **Number of primers** | 2 | 2 | 2 | 2 or 4 | 4 or 6 |
| **Temperature** | 41°C | 30-65°C | 37-42°C | 30-65°C | 60-65°C |
| **Amplification time** | 1-3h | 1-4h | 20-40 min | 1-2h | 1h |
| **Sensitivity (copies of target)** | 1 | 10 | 1 | 10 | 5 |
| **Tolerance to contaminants** | Medium | Low | High | Low | High |

When developing a nucleic acid test with good sensitivity and low cost, a technique with the fewest number of primers would be the most interesting, since primers tend to be expensive. Those are the downsides of SDA and LAMP that require more than two primers. Regarding temperature requirements at which the amplification is taking place, NASBA and LAMP both require temperatures that are higher than the human body (37°C), which requires higher energy consumption and results in higher costs. The methods that show better sensitivities are NASBA and RPA, as depicted in **Table 2**. To sum up, the method that seems to fill most of the requirements is RPA, considering that it also has

the lowest time of amplification, the highest tolerance to contaminants and that even though the optimal temperature is 37-42°C, the reaction can also take place at ambient temperature. However, it is important to look for possible non-specific amplifications, especially when short RPA primers are used [44], [59].

RPA is an amplification method that amplifies target DNA by using a DNA polymerase, a recombinase and Single-Stranded DNA-Binding proteins (SSBs) to prevent re-annealing. It promotes primer binding by using recombinase enzymes to template and strand exchange [**Figure 7**] [60]. With recent developments, RPA sensitivity and specificity are very close to that of PCR. Jiang *et al.* did a study on the detection of *M. pneumoniae*, comparing the sensitivity and specificity of RPA to real-time PCR. In all the samples, RPA gave a detection rate of 48.4%, while PCR had 46.3%, which shows that RPA gives similar results in terms of sensitivity. Moreover, compared to PCR, RPA had 100% of sensitivity and 96.2% of specificity [61].

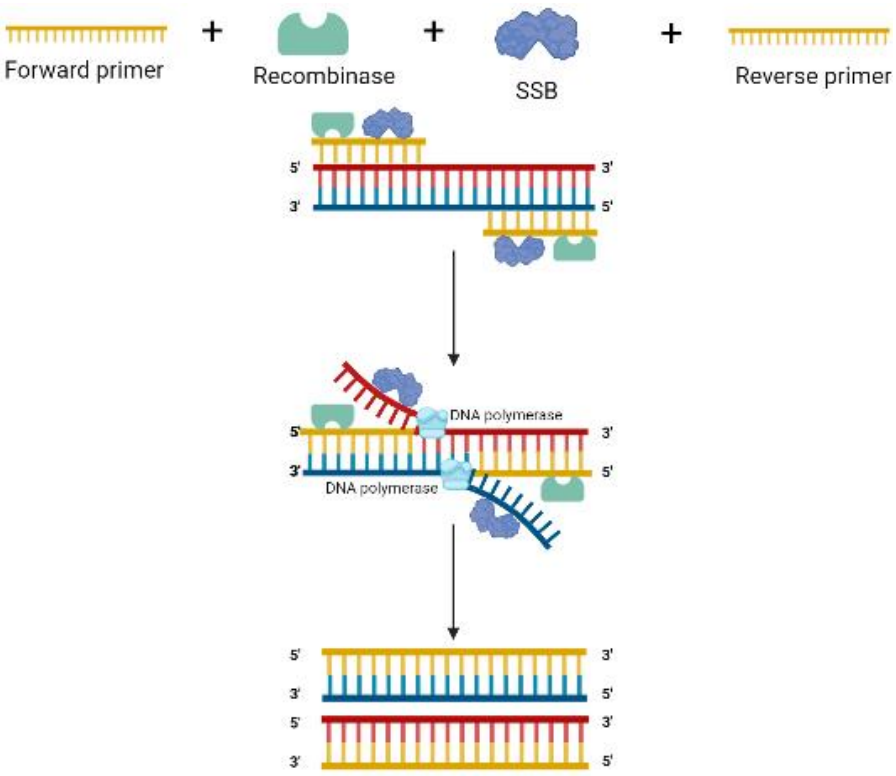


**Figure 7: Process of Recombinase Polymerase Amplification.** Firstly, the recombinase protein binds to the primers to form a complex that will allow strand displacement of the homologous sequence from the target to the primer. The single-stranded DNA-binding proteins (SSBs) will stabilize the opened strand. Then, in the presence of dNTP, a DNA polymerase will bind to the 3'end of the primers and elongate them.

RPA has been developed by Piepenburg *et al.* [62] from the company TwistDx which is also the company that commercializes the RPA kits to enable the amplification. Different kits can be used depending on the type of detection of the RPA product. Amongst the most popular kits, the TwistAmp® nfo kit (TwistDx, UK) is the most convenient for RPA product detection by lateral flow assay. This kit can

also be reproduced by using the TwistAmp® Liquid basic kit (TwistDx, UK) and an endonuclease IV (nfo). The nfo will recognize and cleave the abasic residue (THF) on the probe that contains an emitting fluorophore. The fluorophore detaches from the 3'end part that possesses a blocker that is blocking the elongation, and this detachment will help the integration into the amplification product through the Bsu polymerase that will extend the 3'end (**Figure 8)** [63]. Then the primer containing the 5'Biotin will form with the labelled probe a double labelled amplicon that the LF strip will capture either the biotin or the FAM, depending on the type of LF strip used [64].

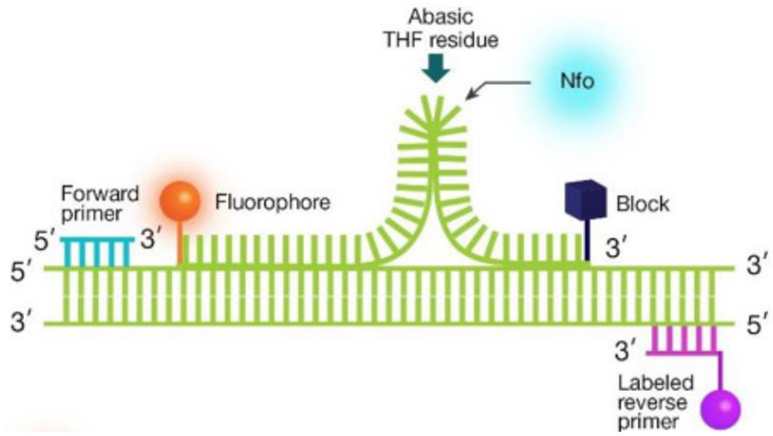


**Figure 8: The mechanism of the nfo.** The nfo is recognizing the abasic THF residue and cleaves it. This will cause the fluorophore (in orange) to be separated from the blocker present at the 3'end (blue). This blocker was blocking the elongation, adapted from [63].

The TwistAmp® Liquid exo kit (TwistDx, UK) uses fluorescence detection either by real-time detection on the fluorometer or by fluorescence microscopy. The exonuclease III contained in the RPA kit, will recognize the THF site, and cleave the probe between the fluorophore and the quencher, which will allow the fluorophore to emit its fluorescence and will allow either the monitoring of the real-time fluorescence in the fluorometer or to see the fluorescence by microscopy [65].

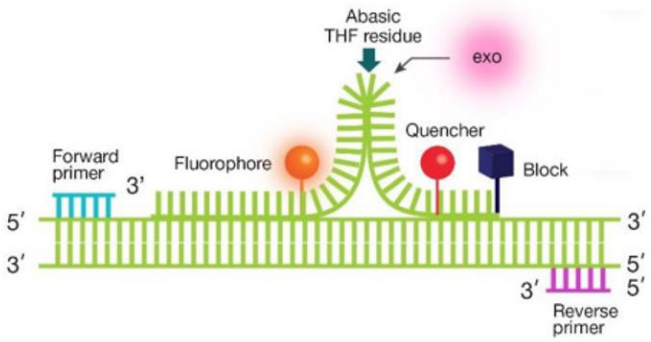


**Figure 9: The mechanism of the exo.** The exonuclease recognises the abasic THF residue and will cleave it. This will cause the fluorophore (in orange) to be separated from the blocker present at the 3'end (blue) and the quencher (red). The separation of the quencher from the fluorophore will allow the fluorophore to emit fluorescence, adapted from [63].

When designing RPA primers and probes, and following the guidelines from TwistDx (Cambridge, UK), a high number of repetitions of certain nucleotides should be avoided and a sequence with a GC content between 30-70% should be the target [65]. As mentioned above, 2 types of RPA probes can be used: an exo probe for real-time detection and an nfo probe for detection via LF assay. Like standard PCR, the RPA product can also be detected when no probe is included, using agarose gel [64][66][67]

The products of amplification can be detected by microfluidic devices and lateral flow dipsticks. Nowadays, 17 years after the publication of the paper describing RPA for the first time, this technique is the most widely used in combination with universal lateral flow assays, as it represents 36.8% of the methods used, followed by LAMP with 28.3%, then CRISPR-Cas technologies with 11.8% and then PCR with 11.5% [66].

#### *1.4.4.4 RPA-LFA (Lateral Flow Assay)*

Lateral flow assays have gained significant popularity in recent years due to their rapid and versatile detection capabilities. They are widely used for various applications, including virus detection after RPA. LF strips are paper-based platforms that utilize colourimetric detection for the qualitative or quantitative analysis of target analytes. These strips are typically incorporated into a compact device and can provide results within approximately 30 minutes. The analytes that can be detected using lateral flow strips include antibodies [67], antigens [68] and amplification products [69]. This versatility allows for the detection of a wide range of biological molecules.

LF strips find applications in various fields, such as veterinary medicine, food safety, toxin detection, water pollutant monitoring, and the diagnosis of human diseases [70]. They offer several advantages, including affordability, rapidity of performance, independence from laboratory facilities, ease of use (no requirement for trained scientists), and a long shelf-life.

Overall, lateral flow strips have become a popular choice for rapid and efficient detection across various fields, thanks to their ability to deliver reliable results in a user-friendly manner.

The development of LFA strips can indeed be challenging, and the choice of the labelling probe plays a crucial role in their performance. Several types of nanoparticles are commonly used as labelling probes, including Gold Nanoparticles (AuNP), Latex particles, magnetic nanoparticles, quantum dots, carbon nanoparticles (CNP), Silica, and europium nanoparticles. These nanoparticles are conjugated with specific biomolecules to enable detection [71].

LFA has been successfully applied to detect various viruses, such as the hepatitis B virus [72], the Epizootic haemorrhagic disease virus, the Palyam serogroup virus [73], respiratory syncytial virus [74] and Alfalfa mosaic virus [75]. When it comes to nucleic acid detection, two labelling probes commonly used in LFA are AuNP and CNP. The selection of the appropriate labelling probe is crucial to ensure sensitive and specific detection in LFA. Factors such as the target analyte, sensitivity

requirements, and compatibility with the detection system need to be considered during the development process.

#### 1.4.4.4.1 Gold Nanoparticles (AuNP)

AuNP-based systems have indeed been extensively explored and are emerging as a prominent element in nanotechnology-based pathogen detection. This preference is mainly due to the unique physicochemical properties exhibited by AuNP and their suitability for biomolecular assays. The distinct properties of AuNPs, such as their excellent stability, biocompatibility, and ease of functionalization, make them ideal for various applications in pathogen detection. These nanoparticles can be easily conjugated with specific biomolecules, such as antibodies or nucleic acids, to create robust and sensitive detection systems. AuNPs exhibit strong optical properties, particularly in the visible range, which allows for straightforward colourimetric detection. The aggregation or dispersion of AuNPs in the presence of a target pathogen leads to noticeable colour changes, enabling visual or spectrophotometric detection. This colourimetric readout simplifies the interpretation of results, making it accessible even to non-experts [76]. This type of strip will be called strip A in this work. The mechanism of the AuNP strip is displayed in **Figure 10. A**, where the sample pad contains AuNP conjugated with anti-FAM antibodies (Ab) and coated with rabbit serum. When the sample is applied to the sample pad, the FAM present on the product of amplification will bind to the anti-FAM Ab (antibodies) which will give it a pink-red colour from the AuNP. With the addition of the running buffer to the sample pad, the product of amplification will run through the LFA strip, passing by the test line (T) that contains streptavidin while binding to the biotin present in the sample. This will immobilize on the test line the amplicons from the product of amplification. The remaining buffer and AuNP will continue flowing through the strip and reach the control line that contains anti-rabbit Ab which will bind to the rabbit serum coating the AuNP. Then the rest of the buffer will reach the absorbent pad.

#### 1.4.4.4.2 Carbon Nanoparticles

Carbon nanoparticles (CNP) are inexpensive carbon materials derived from candle soots, and can serve as a reliable fluorescent sensing platform for nucleic acid detection. The CNPs demonstrated high selectivity, even down to single-base mismatches. However, it should be noted that CNPs below 10 nm in size are not suitable candidates for a fluorescent sensing platform in nucleic acid detection applications. This is because these small CNPs exhibit strong photoluminescence emission that interferes with the detection process [77]. The CNP LFA strip will be called strip B in this work for confidentiality reasons. The global detection mechanism for LFA strips that use CNPs is displayed in **Figure 10. B**. In summary, the sample pad contains CNPs conjugated with anti-biotin antibodies (Ab) and coated with mouse serum. The sample or the product of amplification is loaded in running buffer in the sample pad. The product of amplification will run through the LFA strip, passing by the test line (T)

that contains anti-FAM Ab that will bind to the FAM present on the sample. This will immobilize on the test line the amplicons from the product of amplification. The other DNA strand labelled with biotin that is present on the dsDNA product of amplification will bind to the anti-biotin Ab, which will give it a grey colour from the CNPs. The remaining buffer and CNP will continue flowing through the strip and reach the control line that contains anti-mouse Ab which will bind to the mouse serum. Then the rest of the buffer will reach the absorbent pad.

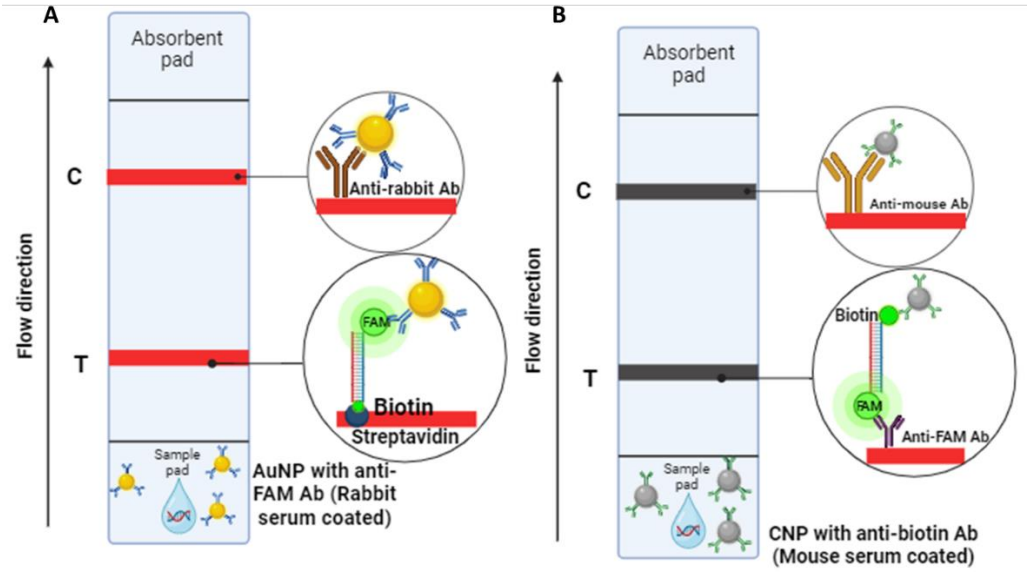


**Figure 10: Main types of lateral flow assay strips for nucleic acid detection.**

### *1.4.4.5 Fluorescence microscopy*

Fluorescence microscopy enables the detection of samples containing a fluorophore, such as FAM, which is commonly for nucleic acid detection. When a sample is exposed to intense light, the fluorophore absorbs the photons, leading to its excitation. After excitation, the fluorophore emits light of lower energy and longer wavelengths, allowing the analyte under analysis to be observed through a camera. To visualize the fluorescence, excitation, and emission filters are combined to select the correct excitations and emission wavelengths. This filter effectively separates the surrounding lights from the specific wavelength emitted by the fluorophore [78].

### 1.4.5 Point-of-care testing

**Table 3** displayed a non-exhaustive list of main blood-based rapid testing technologies currently available. The main goal now would be to achieve a technology that would have a high sensitivity and specificity like RT-LAMP, while being as fast and not invasive as the SD Bioline Dengue Duo test. Moreover, there is a need for the less invasive method possible like the Panbio Dengue Early ELISA kit that only requires capillary blood (~30-40 µL) which is less invasive than the RT-iiPCR with POCKIT nucleic acid analyzer that requires veinous blood (~130 µL) [79]. Also, the sampling of veinous blood requires trained personnel while the sampling of a drop of capillary blood is easy to do without training. The goal technology to achieve would also need to be with low costs like the SD Bioline Dengue Duo (~28€/test [80]) compared to the RT-iiPCR with POCKIT nucleic acid analyzer (~2000€ equipment that can run multiple tests [81]). Another important requirement is the time of the assay, the goal is to have a fast assay like the SD Bioline Dengue Duo which has a 15-20 min assay time [82]compared to the Panbio Dengue Early ELISA kit that has an assay time of 2h10 [83]. The element described in the previous chapter 1.4.4 can be used to achieve this goal by POC testing. The need for less invasive and quicker blood analysis to deliver quantitative measurement of blood parameters is becoming more and more important while remaining affordable and sure with good sensitivity and specificity.

**Table 3: Current advances on Dengue virus rapid testing.**

| Reference | Technology | Target | Sample type | Time | Sensitivity (%) | Specificity (%) |
|---|---|---|---|---|---|---|
| Go *et al.*, 2016 [84] | RT-iiPCR with POCKIT nucleic acid analyzer | 3'UTR gene | Blood (serum), veinous blood | 60 min | 90.5 | 98.3 |
| Neeraja *et al.*, 2015 [85] | RT-LAMP | NS1 gene | Blood (serum and plasma) | 70 min | 94.6 | 100 |
| Tan *et al.*, 2014 [86] | RT-PCR with microfluidic lab-on-a-chip | NS5 gene | Blood (serum) | 4h | 85 | 100 |
| Manoor Anand *et al.*, 2016 [83] | Panbio Dengue Early ELISA kit | NS1 antigen | Blood (serum), capillary blood | 2h10 | 96.9 | 53 |
| Piedrahita *et al.*, 2016 [82] | SD Bioline Dengue Duo | IgM/IgG antibodies + NS1 antigen | Blood (serum), capillary blood | 15-20 min | 30.8% | 73.3 |

## 1.5 Objectives

The main goal of this master thesis project was to develop a test to detect the Dengue virus that is at the same time fast, affordable, non-invasive, rapid, and reliable. In this work, we pave the way and demonstrate the development of a point-of-care nucleic acid test requiring only a simple drop of blood. Eliminating the thermal cycler to save costs is key, to decrease costs and implementing an isothermal amplification method is the best approach. From the isothermal amplification techniques, RPA presented, in theory, the required conditions for target temperature, assay duration and sensitivity. The main end goal is to carry the whole RPA amplification and detection in a microfluidic cartridge. An already existing cartridge developed by the company biosurfit was used, in the form of a disc that is using centrifugal microfluidics for the mixing of the reagents. These RPA results will be compared to qPCR which will serve as a reference test, the latter will be detected by real-time fluorescence and agarose gel electrophoresis. Two possible detection modules will be tested: colourimetric and fluorescence detection. The colourimetric detection will leverage on a lateral flow assay strip using nanoparticles, that will be integrated directly into the microfluidic disc, while the fluorescence detection will be made in the

detection chamber of the disc by a dedicated hardware device. The development of this work will mainly focus on the Dengue virus, and once the experiments prove that the project is possible and conclusive, it will be possible to adapt this test easily to detect Chikungunya and Zika viruses.

# 2. MATERIALS AND METHODS

## 2.1 Entities

This work was carried out in the R&D Department of the company biosurfit, with some steps carried out in the clean room environment of the production line of the Production Department.

## 2.2 Virus and design of DENV-specific primers and probes

The target is a part of DENV2 (GenBank™ accession number KM204118) New Guinea C (NGC), 3'UTR gene (10273-10723) (see the complete sequence of 3'UTR gene and of the genome of DENV2 NGC in the supplementary material) for experiments PCR1, RPA1, PCR2 and RPA2 (Position in genome covered: 10447-10687) [87]. For experiments RPA3, PCR3, and PCR4, the target is part of DENV2 (KM204118) NGC, 3'UTR gene (10273-10723), englobing the whole gene from position 10273 to 10723.

The targets were supplied as gBlock™ gene fragments by Integrated DNA Technologies (IDT) (Coralville, USA), that mimic a cDNA (sequences presented below) of the RNA sequences of interest. In summary, the gBlock™ worked as an RNA virus model after a reverse transcription step.

DNA of the amplification target sequence for experiments PCR1, RPA1, PCR2 and RPA2:

**5'GAAATTAATACGACTCACTATAGGG**AAATCTGGGAGGCCACAAACCATGGAAGCTGTACGCATG
GCGTAGTGGACTAGCGGTTAGAGGAGACCCCTCCCTTACAAATCGCAGCAACAATGGGGGCCCA
AGGTGAGATGAAGCTGTAGTCTCACTGGAAGGACTAGAGGTTAGAGGAGACCCCCCCAAAACAAA
AAACAGCATATTGACGCTGGGAAAGACCAGAGATCCTGCTGTCTCCTCAGCATCATTCCAGGCAC
AGAACGCCAGAAAATGGAATGGTGCTGTTGAATCAACAGGTTCT**3'**

DNA of the amplification target sequence for experiments RPA3, PCR3 and PCR4:

**5'**AAGGCAAAACTAACATGAAACAAGGCTAGAAGTCAGGTCGGATTAAGCCATAGTACGGAAAAAAC
TATGCTACCTGTGAGCCCCGTCCAAGGACGTTAAAAGAAGTCAGGCCATTACAAATGCCATAGCTT
GAGTAAACTGTGCAGCCTGTAGCTCCACCTGAGAAGGTGTAAAAAATCTGGGAGGCCACAAACCA
TGGAAGCTGTACGCATGGCGTAGTGGACTAGCGGTTAGAGGAGACCCCTCCCTTACAAATCGCAG
CAACAATGGGGGCCCAAGGTGAGATGAAGCTGTAGTCTCACTGGAAGGACTAGAGGTTAGAGGA
GACCCCCCCAAAACAAAAAACAGCATATTGACGCTGGGAGAGACCAGAGATCCTGCTGTCTCCTC
AGCATCATTCCAGGCACAGAACGCCAGAAAATGGAATGGTGCTGTTGAATCAACAGGTTCT**3'**

In the first sequence in bold appears a T7 promotor sequence that is not part of the DENV2 NGC genome. This promoter sequence could be used for CRISPR detection, which was the original idea at the beginning of the project but is not presented here in this work.

RPA and PCR/qPCR primers and probes were designed to amplify by RPA, PCR/qPCR, respectively, the part of the 3'UTR gene, a high-conserved region of DENV2 NGC strain, predefined for the study by the project's partner the Instituto de Patologia e Imunologia Molecular da Universidade do Porto (IPATIMUP) (Porto, Portugal). Primers PCR1 and RPA1 were defined by IPATIMUP in a first study using the database VIPR and CATCH software to align the sequence in the study and select the primer regions. Primer pairs PCR2, RPA2, and probes PCR1 qPCR1, RPA1, PCR-RPA(LF)2 (**Table 4**) were defined using the Primer Express software (ThermoFisher) taking into account the guidelines mentioned

in chapters 1.4.4.1 and 1.4.4.3. In addition, the Tm has also been checked according to the experimental design for PCR experiments [49] with the software PerlPrimer v1.1.21 [88]. The already existing sequences for RPA3 were generated by Teoh *et al.*, 2015 [89]; for PCR3 were generated by Alm *et al.*, 2014 [90] and for PCR4 were generated by Xi *et al.*, 2019 [91]. For qPCR, we used a TaqMan® probe, labelled at 5' with a fluorescent dye 6-Carboxyfluorescein (6-FAM) and a 3' quencher (Black Hole Quencher-1 (BHQ-1)).

All nucleotides in the table **Table *4*** had a stock concentration of 100 µM and were purified by HPLC. FAM fluorophore displayed in the table, has an excitation peak at 493 nm and an emission peak 517 nm [92].

**Table 4: Nucleotide sequences.**

| Name | Sequences (5'- 3') | 5'end mod | 3'end mod | Tm (°C) | GC (%) | Supplier |
|---|---|---|---|---|---|---|
| Fw_primer PCR-RPA1 | CCTTACAAATCGCAGCAACAATGGGGG | None | None | 68.9 | 51 | StabVida |
| Rv_primer PCR1 | CTCTGGTCTCTCCCAGCGTCAATATG | None | None | 66.8 | 53 | StabVida |
| Rv_primer RPA1 | CTCTGGTCTCTCCCAGCGTCAATATG | Biotin | None | 66.8 | 53 | StabVida |
| Fw_primer PCR-RPA2 | CCTTACAAATCGCAGCAAC | None | None | 57.8 | 47 | Eurogentec |
| Rv_primer PCR2 | TTC CCA GCG TCA ATA TGC TG | None | None | 61.0 | 50 | Eurogentec |
| Rv_primer RPA2 | TTC CCA GCG TCA ATA TGC TG | Biotin | None | 61.0 | 50 | Eurogentec |
| Fw_primer PCR3 | GCA TAT TGA CGC TGG GAG AGA | None | None | 62.5 | 52 | Eurogentec |
| Rv_primer PCR3 | TTC TGT GCC TGG AAT GAT GCT G | Biotin | None | 63.7 | 50 | Eurogentec |
| Fw_primer PCR4 | TGC TGC CTG TAG CTC CAT CGT | None | None | 66.5 | 57 | IDT |
| Rv_primer PCR4 | GAA CCT GTT GAT TCA ACA GCA CCA | Biotin | None | 64.3 | 45 | IDT |
| Fw_primer RPA3 | CAG CAT ATT GAC GCT GGG AAA GAC CAG AGA TC*C | Biotin | None | 71.6 | 51 | IDT |

| | | | | | | |
|---|---|---|---|---|---|---|
| Rv_primer RPA3 | GAA CCT GTT GAT TCA ACA GCA CCA TTC CAT TT*T | None | None | 68.6 | 39 | IDT |
| Probe_PCR1 | GAGATGAAGCTGTAGTCTCACTGGAAGGACTAGATGTTAGAGGAGACCCCCC | FAM | C3 | - | - | Eurogentec |
| Probe_qPCR1 | GAGATGAAGCTGTAGTCTCACTGGAAGGACTAGATGTTAGAGGAGACCCCCC | FAM | TAMRA | - | - | Eurogentec |
| Probe_RPA1 | GAGATGAAGCTGTAGTCTCACTGGAAGGACTAGA**(dT-FAM)(THF)(dT-BHQ1)**TAGAGGAGACCCCCC | None | C3 | - | - | Eurogentec |
| Probe_PCR-RPA(LF)2 | AC TGG AAG GAC TAG AGG TTA GAG GAG | FAM | C3 | - | - | Eurogentec |
| Probe_qPCR3-4 | CAG AGA TCC TGC TGT C | FAM | BHQ | 67 | 56.3 | IDT |
| Probe_PCR3-4 | CAG AGA TCC TGC TGT C | FAM | C3 | 67 | 56.3 | IDT |
| Probe_RPA3-1 | CCA TTT TCT GGC GTT CTG TGC CTG GAA TGA TG/**iFluorT**/ TG/**idSp//iBHQ-1dT**/ GAG ACA GCA GGA T | None | C3 | 69.4 | 49 | IDT |
| Probe_RPA3-2(LF) | CCA TTT TCT GGC GTT CTG TGC CTG GAA TGA TGC TG/**idSp**/A GAG ACA GCA GGA TC | FAM | C3 | 69.8 | 52 | IDT |
| Probe_membrane | CATATTGACGCTGGGAGAGACCAGAG | None | None | 69.4 | 49 | IDT |

*(*) is for phosphorothioate linkages to inhibit exonuclease degradation, dT-FAM: thymidine nucleotide carrying fluorescein, iFluorT = thymine base modified with fluorophore, idSp: tetrahydrofuran basic site mimic (THF residue), dT-BHQ1: thymidine nucleotide carrying black hole quencher.*

## 2.3 Validation of the Lateral Flow Assay (LFA)

### 2.3.1 Validation of the strip for LFA by study of LoD

#### *2.3.1.1 Detection*

First, the determination of the most appropriate LFA strip for the project was decided between strip A (based on AuNP) and strip B (based on CNP). A calibration curve was created with concentrations ranging from 0 to 330 nM for strip A and from 0 to 1 nM for strip B, with three replicas for each concentration. The supplier's recommended protocol was followed: 5 µL of product of amplification followed by 70 µL of TBS (Tris-Buffered Saline) lateral flow assay buffer supplied with strip A called buffer A, were applied on the sample pad. The synthetic dsDNA mix used contains Rv_PrimerRPA1 and Probe_membrane, presented in **Table *4***. Those two oligonucleotides were mixed with the desired concentration for each assay. The 5 µL of the synthetic dsDNA mix was then mixed with 70 µL of buffer A supplied with the membrane. The membranes were placed in lateral flow cassettes and the total mix was applied to the sample pad of the membrane. Results were captured after 15 min by Leica DMS300 Digital Microscope System (Leica Microsystems, Germany) with a 7.5x magnification and light at the maximum. The images were processed with the software ImageJ (National Institutes of Health, USA).

#### *2.3.1.2 Image processing*

The image processing method is adapted from Kaminski *et al.*, 2020 [93]. The colour channels of the images were split (RGB) and the Green channel was kept for analysis under 8-bit. The intensity of the test band was measured and normalized as the mean grey value of the test band divided by the mean grey value of the background. Another calibration curve of strip A was made for comparison with a normalization of the intensity of the band with the mean grey value of the test band divided by the mean grey value of the control band exactly like in Kaminski *et al.*, 2020.

#### *2.3.1.3 Data analysis*

The data analysis was performed with the software GraphPad Prism 8.0.1 (GraphPad, USA). A non-linear regression analysis was chosen, with a semi-log line equation in the range of the slope of the curve. Then the best-fit values of the $Y_{intercept}$ and of the slope are retrieved to allow the calculation of the limit of detection (LoD) via the formulas [94]:

$$LOD = Y = (mean\ of\ blanks) + (3.3(\sigma))$$

**Equation 1: LoD calculation.**

Where:

Mean of blanks = the mean value of the curve at 0 nM

σ = standard deviation of the blank (at 0 nM)

Since the equation of the graph is:

$$Y = Yintercept + slope * \log(X)$$

$$\Leftrightarrow \log(X) = \frac{Y - Yintercept}{Slope}$$

$$\Leftrightarrow X = 10^{\log(x)}$$

**Equation 2: Retrieving the X value corresponding to the LoD.**

## 2.3.2 Integration of the LFA in the microfluidic disc

### *2.3.2.1 Microfluidic disc*

The disc layout used is the spinit® COVID-19 Antibody point-of-care blood test (**Figure 11**), which is a disc primarily polycarbonate based. The disc was originally designed to be loaded with 30 µL of capillary blood that is subject to plasma separation by centrifugal force inside the spinit equipment. This procedure can extract 5.7 µL of plasma that will posteriorly reach a lateral flow membrane specifically selected for this test.

The volume definition for the subsequent assays was this way defined as 5.7 µL for direct loading on lateral flow tests performed outside the disc and 30 µL for assays performed inside the disc.

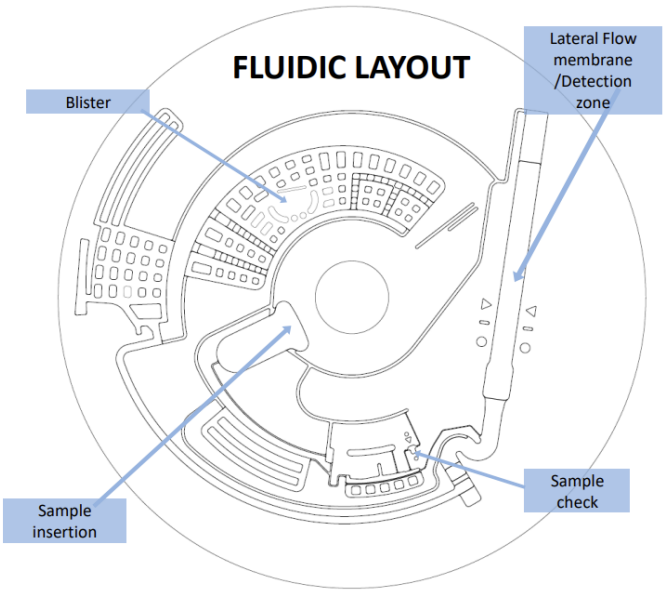


**Figure 11: Microfluidic layout from the COVID-19 disc obtained from Biosurfit.**

The rotation of the disc is ensured by a centrifugation protocol (not displayed here for confidentiality) using a standard CD-ROM drive featuring in the spinit® instrument (biosurfit, Portugal)

(**Figure 12**). The instrument contains various detection methods due to the variety of assays that can be performed with this instrument, including a digital camera (**Figure 13**) [95].


**Figure 12: spinit® instrument** [95].

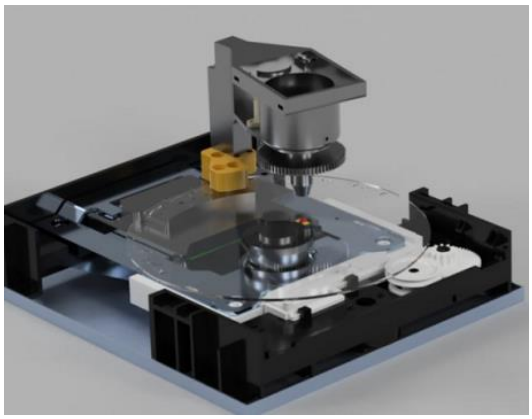

**Figure 13: Set-up for analyte detection by digital camera inside the spinit® instrument** [95].

### 2.3.3 dsDNA detection by direct dispense on LFA strip integrated on disc, without disc rotation

#### *2.3.3.1 Assay*

This first assay on the disc was performed without rotation, with the LFA strip A integrated into the disc. The reagents are directly applied on the S shape of the microfluidics, located directly before the LFA strip (see **Figure 14** - Sample highlight). It is important to note that from this assay until the end of chapter 3.2, the strips A used are different from the ones from the previous assay. Indeed, as the uncut sheet was not commercially available, the strips were purchased already precut as dipsticks. The initial tests on the strips were done with 5 µL of synthetic dsDNA mix and 70 µL of buffer (as per the supplier's recommendations). However, since inside the disc, the volumes of sample and buffer reaching the membrane are 5.7 µL and 79 µL, respectively, those were the proportions tested in this assay. Furthermore, the sample concentration tested was 1 nM. The same synthetic dsDNA mix was used as

in chapter 3.1.1. Two different buffers were tested here, buffer A (that was supplied with strip A) and buffer B (that was supplied with strip B).

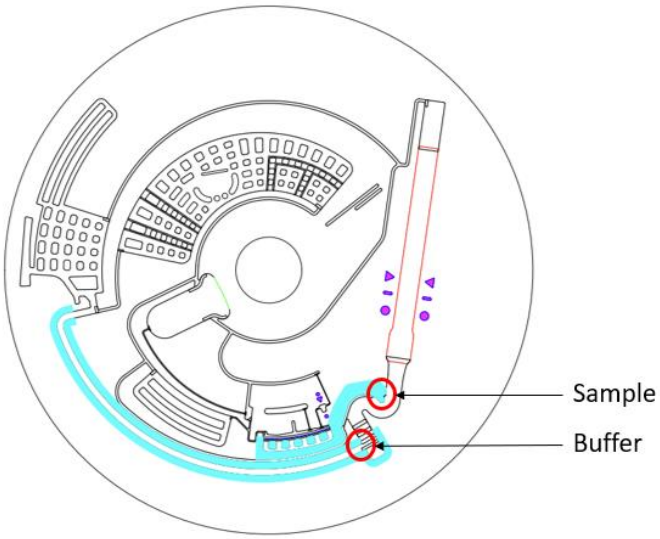


**Figure 14: Direct dispense of the reagents on the S membrane.**

Two configurations of strip A were tested: configuration A where 0.7 cm was cut on the sample pad and 0.5 cm was cut on the absorption pad and configuration B where 1.2 cm was cut entirely on the absorption pad (**Figure 15**).

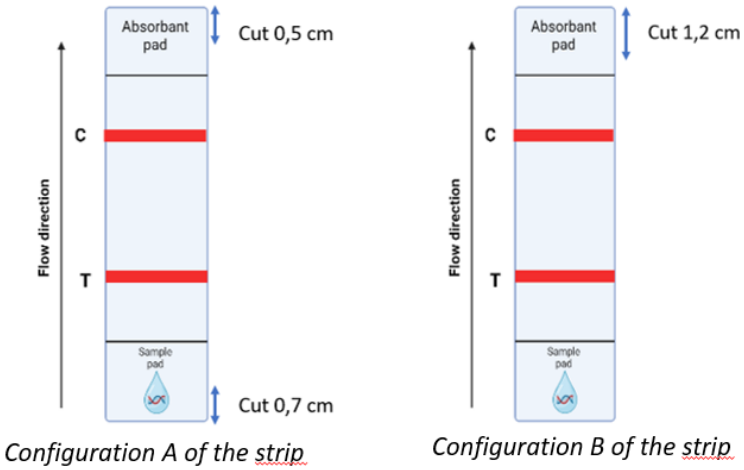


**Figure 15: Different configurations of the strip for the assay.**

Four strips of each configuration were prepared and cut with a blade. Then each strip was carefully placed in the disc with an S membrane with the help of tweezers. The discs were closed with a specific tape that fits the design of the disc (tape of the COVID-19 disc) and the closed disc was put under a mechanical press (IMESIF LDA, Portugal) (**Figure 16**) to apply the required pressure for correct disc sealing, with a vacuum of -0.71 Bar and an applied strength of 495.4 Kg. Then with a blade, holes

were made in the appropriate places of the disc for the injection of the buffer and of the synthetic dsDNA mix for each disc.

**Figure 16: Mechanical press to enhance the bonding of the closing tape.**

In total, four conditions were tested: configuration A with buffer A, configuration A with buffer B, configuration B with buffer A and configuration B with buffer B. Each condition was done in duplicate. A picture was taken with the Leica DMS300 Digital Microscope System (Leica Microsystems, Germany) at t0 (before injecting the synthetic dsDNA mix and the buffer) and at t15 (15 min after the injection).

### *2.3.3.2 Image processing*

Image processing and data analysis were optimized and the method selected is hereby described. Firstly, the RGB picture was imported to ImageJ and the colour channels were split. The picture from the Green Channel was kept for analysis. A straight segment was drawn from left to right in the middle of the membrane. Then the plot profile analysis was displayed. The cursor was placed on top of the deepest point of the deep for each line (**Figure 17**). The X value for the t15 will be used for the t0 to place the cursor on the same X value to retrieve its Y value (**Figure 18**). Then the Y(X) values of the t0 and t15 corresponding to the same X value will be compared for analysis. This analysis was performed for both the test and the control lines.

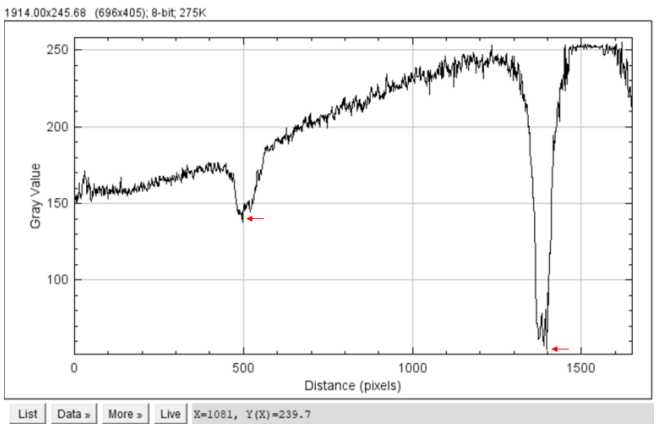


**Figure 17: Plot analysis at t15.**

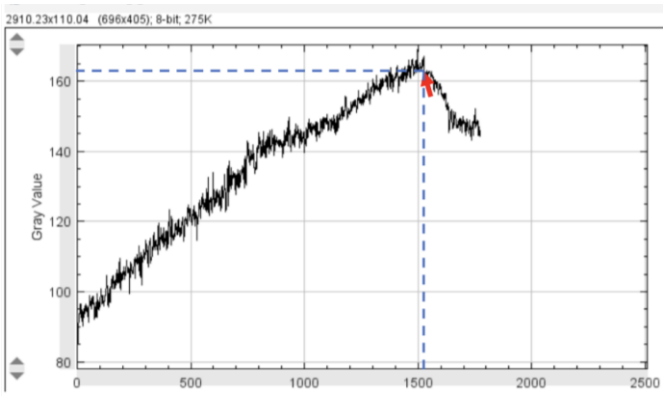


**Figure 18: Plot profile while retrieving the Y(X) value at t0.**

Then, the following formulas were used to determine the Mean grey value of the test:

$$Test\ line\ value = Point\ value\ for\ the\ test\ line\ at\ t0 - Point\ value\ for\ the\ test\ line\ at\ t15$$

$$Control\ line\ value = Point\ value\ for\ the\ control\ line\ at\ t0 - Point\ value\ for\ the\ control\ line\ at\ t15$$

$$Ratio = \frac{Test\ line\ value}{Control\ line\ value}$$

**Equation 3: Ratio quantification test line,** the test and control lines values are calculated using the value at t0 subtracted by the value at t15. Then the test and control lines values obtained are divided to obtain the ratio.

This ratio is the value used for the quantification of the test line for all the assays.

#### *2.3.3.3 Calibration curve*

After selecting the best conditions from the previous assays, a calibration curve was made for concentrations ranging from 0 nM to 150 nM, with triplicates for each concentration. The LoD was calculated with the same method as the one described in chapter 3.1.3. For this assay, it was decided to add 30 µL of buffer to the volume used before, since the assay seemed to lack running buffer in the previous experiment. Consequently, 109 µL of buffer A was used for this and the following assays.

### 2.3.4 dsDNA detection in LFA strip integrated on disc, using disc rotation for liquid control

For this assay, the protocol was very similar to the previous one except that the dispense of the buffer and the synthetic dsDNA mix are in the adequate chambers as highlighted in **Figure 19**. The 32 µL of synthetic dsDNA mix was loaded in the sample inlet and 109 µL of buffer A was loaded in the buffer inlet. After sample loading, the disc was inserted into a dedicated device called strobeit, that is performing the centrifugation of the cartridge (**Figure 20**). The strobeit consists of a rotor controlled by a computer to execute the rotations protocols required for each assay and rotate the disc, and an acquisition system coupled with a stroboscope that allows for an image of an area of interest to be captured for each revolution of the disc. In this case, the required centrifugation protocol with a duration of 3-5 min allowed the movement of liquids inside the disc, the mix of the sample and buffer, and allowed them to reach the S membrane. After the end of the rotation, a waiting time of 30 min was necessary for the reagents to go through the S membrane and the LFA strip. A first test was done with dyes (blue to represent the sample and yellow to represent the buffer), to ensure that the rotation protocol was correct. Then a calibration curve was made with the synthetic dsDNA mix and the buffer, at concentrations ranging from 0 nM to 20 nM with three replicas.

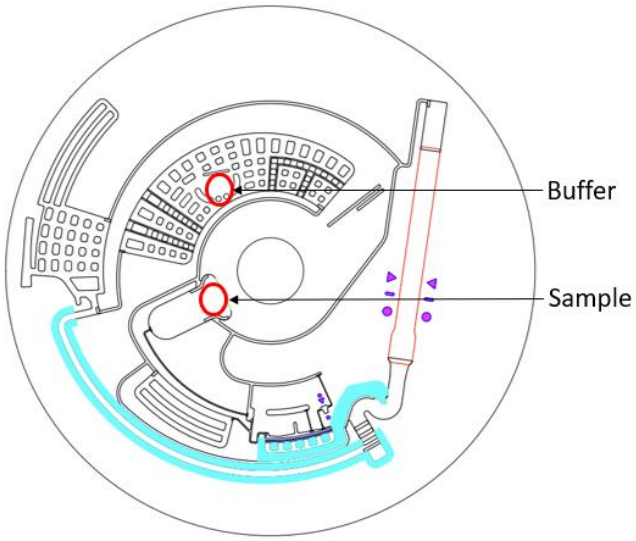


**Figure 19: Dispense of the reagents on the disc.**

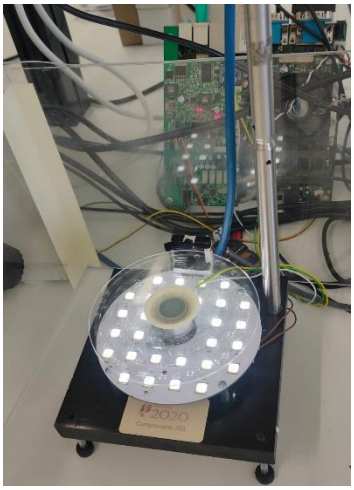

**Figure 20: The strobeit**, that reproduces the rotation that takes place in the spinit® instrument.

## 2.4 Validation of Real-time PCR (qPCR) and PCR protocol and primers for comparison with the RPA assay

All the assays were performed under the Aura mini vertical laminar flow cabinet (Bioair, Italy). The DENV qPCR assay was carried out in a 25 µL reaction mixture in a PCR tube that contains 5 µL cDNA template (or nuclease-free water for the NTC (Non-Template Control)), 20 µL of master mix, that contains 12.5 µL of Master Mix solution (Maxima Probe/ROX qPCR Master Mix (Thermofisher scientific, USA)), 0.2 µM of probe, Fw_primer and Rv_primer (various concentrations depending on the assay with a final concentration of 0.8 µM and nuclease-free water (Thermofisher scientific, USA) until the solution reaches 20 µL and PBS.

The amplification and detection of the amplicon were performed in a Gentier 48E Real-time PCR System (Xi'an Tianlong Science and Technology Co., China). All samples were tested in duplicates and NTC were done in duplicates for each experiment. The starting concentration of cDNA was measured in copies/mL. Multiple assays were run to optimize the conditions of the qPCR assay.

### 2.4.1 qPCR1/PCR1

The following assays of this section were conducted with the primers Fw_primerPCR-RPA1 and Rv_primerPCR1.

#### *2.4.1.1 qPCR1.1*

The master mix contains 0.8 µM of Rv_primer and 0.8 µM of Fw_primer. The thermal cycle's parameters were the following: Preincubation step at 50°C for 2 min, then 40 cycles of a 3-step amplification of 10 min at 95°C, 15s at 95°C (where the fluorescence is being read) and 1 min at 56°C.

#### *2.4.1.2 qPCR1.2*

The protocol is the same as the one for qPCR1.1, but an additional elongation step at 72°C for 30 sec was added at the end of the cycle. Additional tests have been made with a primer's concentration of 0.6 µM for both since the primer's concentration recommended for PCR is within the range of 0.3-1 µM and a high primer concentration can contribute to nonspecific amplification [49], so optimizing the assay with a lower primer concentration can contribute to better results.

#### *2.4.1.3 qPCR1.3*

The master mix contains 0.4 µM of each primer for one assay and 0.8 µM for another one. The thermal cycle's parameters were the following: preincubation at 42°C for 5 min, then 10 min at 95°C and then 40 cycles of a 3-step amplification with 30s at 95°C (with fluorescence reading), 1min at 56°C and 30s at 72°C.

#### *2.4.1.4 qPCR1.4*

The master mix contains 0.3 µM of each primer. The thermal cycle's parameters were the following: an initial denaturation at 94°C for 5 min, 40 cycles of a 3-step amplification with 1 min at 94°C, 1 min at 66°C (with fluorescence reading) and 1 min at 72°C. Then a final extension at 72°C for 20 min.

#### *2.4.1.5 PCR1*

The goal of this assay is to amplify the target by conventional PCR and to detect the product of amplification by LFA with strip A. For this matter, the same protocol as for assay qPCR1.4 was used, the only difference is the probe used. Two conditions will be tested: one assay with the probe_PCR1 and another one with the probe_RPA1 with duplicates for each condition, with a target concentration of $10^{10}$ copies/mL, as a smaller target concentration was previously tested but didn't give exploitable results. To concord with the literature that used a total volume of liquid on the LFA strip B of ~ 90 µL, including the product of amplification and the buffer, it was decided for this assay to apply a total volume of 90 µL on the strip (RPA product + buffer) and to apply the entirety of the PCR product on the strip (25 µL). Consequently, the quantity of buffer necessary to reach 90 µL of liquid applied to the strip generates a volume of buffer of 65 µL. Then the protocol for the analysis of the results is the same as in chapter 3.1. A second analysis by agarose gel electrophoresis can be found in the supplementary material (**Figure 47**).

### 2.4.2 PCR2

The shorter primers Fw_primerPCR-RPA1 and Rv_primerPCR1 were tested with Probe_PCR-RPA(LF)2 at $10^4$ and $10^5$ copies/mL by agarose gel electrophoresis and the results can be found in the supplementary material (**Figure 49**).

### 2.4.3 qPCR3-4

The following experiments were done with the PCR_probe3-4 with a concentration of 0.24 µM. The product of amplification was analysed by amplification curve on the Gentier 96E Real-Time PCR System (Xi'an Tianlong Science and Technology Co., Ltd) (fluorometer) and gel electrophoresis post-amplification. The thermal cycle's parameters were the following: Preincubation step at 95°C for 3 min, then 40 cycles of a 3-step amplification of 20s at 95°C, 30s at 60°C (where the fluorescence is being read) and 30s at 72°C. Then an elongation step at 72°C for 5 min.

#### *2.4.3.1 qPCR3-4.1*

This assay was run with Fw_primerPCR3 and Rv_primerPCR3 with a concentration of each primer of 1 µM. This assay is called PCR3.

#### *2.4.3.2 qPCR3-4.2*

This assay was run with Fw_primerPCR4 and Rv_primerPCR4 with a concentration of each primer of 1 µM.

#### *2.4.3.3 qPCR3-4.3*

This assay was run with Fw_primerPCR3 and Rv_primerPCR4 with a concentration of each primer of 1 µM for one assay and 0.8 µM for the other. This assay is called PCR3-4a for the one at 1 µM and PCR3-4b for the assay at 0.8 µM.

#### *2.4.3.4 qPCR3-4.4*

This assay was run with Fw_primerRPA3 and Rv_primerRPA3, with a concentration of each primer of 1 µM. This assay is called RPA3.

#### *2.4.3.5 qPCR3-4.5*

This assay was run with Fw_primerPCR3 and Rv_primerPCR4 with a concentration of each primer of 0.8 µM. The goal is to build a calibration curve with target concentrations ranging from $10^{10}$ to $10^3$ copies/mL with duplicates and two NTC (non-template control). The efficiency of the PCR was calculated using the $R^2$ and slope values with the following formula:

$$E = -1 + 10^{(\frac{-1}{slope})}$$

**Equation 4: Efficiency of the PCR.**

A good, expected efficiency is within the range of 90-110% [96].

### 2.4.4 Agarose gel electrophoresis post qPCR amplification

#### *2.4.4.1 Agarose gel preparation*

1X TBE was prepared by mixing TBE electrophoresis buffer powder (miniPCRbio, USA) with distilled water. 5.1g of powder with 600mL of distilled water makes 600 mL of TBE buffer.

Since the expected lengths of the PCR products are between 21-49 bp, which is particularly small, a 2.5% agarose gel was prepared [97]. For a 60 mL agarose gel, 1.5g of SeaKem® LE Agarose (Lonza, Switzerland) was mixed with 60 mL of 1X TBE buffer. The solution needs to be mixed evenly and then to be heated until boiling and mixed again. This step needs to be repeated until no hair structure can be seen in the mix. The mix was then cooled at room temperature. Then the nucleic acid stain SeeGreen™ 20 000X (miniPCRbio, USA) was added to the gel with a ratio of 1 µL per 20 mL of agarose gel.

#### *2.4.4.2 Gel electrophoresis*

The equipment used for the gel electrophoresis is the GELATO™ electrophoresis and visualization system (miniPCRbio, USA). The support of the gel was put on the casting tray then the combs to make the wells in the gel were placed. The agarose gel was placed in the gel box of the electrophoresis unit until it reached almost the top of the teeth of the comb. Once the gel solidified, the combs were removed vertically and the gel was put onto the electrophoresis tray. The gel box was then filled with 1X TBE buffer with a level of one-third of a finger above the gel while staying below the electric connections. After, 2 µL of 100 bp DNA Ladder N3231S (New England BioLabs, USA) was mixed with 2 µL of Gel Loading Dye Blue (6X) B7021S (New England BioLabs, USA) and the 4 µL of the mix was loaded in the middle lane of the gel. Afterwards, 10 µL of the PCR product was taken and mixed with 2 µL of the blue

dye. 10 µL of this mixture was loaded into the well, and the same process was repeated for each sample. Then the gel was run at 75V for 1h30.

## 2.5 RPA amplification and detection of the RPA product

### 2.5.1 RPA1

For the RPA assays 1, the combination of primers/probe were the following: Fw_primerPCR-RPA1, Rv_primerRPA1, and probe_RPA1 with stock concentrations of 10 µM. The RPA kit used for the assays for chapters 5.1 and 5.2 is the TwistAmp® Liquid exo (TwistDx, UK). The protocol follows the recommendations from the supplier [98]. For one reaction of 50 µL, the master mix was prepared in an Eppendorf tube and contains 25 µL of 2X Reaction buffer, 3.6 µL of dNTPs + 4.6 µL of water (to reach 8.2 µL), 5 µL of 10x Probe E-mix, 2.1 µL of Fw_Primer, 2.1 µL of Rv_Primer and 0.6 µL of Probe. The mix was put in the vortex and briefly spun. Then the 20x Core Reaction Mix that was warmed to room temperature was slowly mixed with a pipette to ensure homogeneity and 2.5 µL of it was added to the tube lid. The tube was mixed with ten full inversions of the tube and briefly spun. To finish, the 50x Exo was mixed with the pipette and 1 µL was added to the tube lid. The tube was mixed by 10x full inversions and briefly spun. The addition of the exonuclease causes the master mix to have a cloudy colour. To finish, 46.5 µL of the master mix was added to a 0.2 mL PCR tube and 2.5 µL of MgOAc (280mM) and 1 µL template cDNA ($10^{10}$ copies/mL) were added to the tube lids. DNA and MgOAc should be kept separate in the tube lid prior to spin-down to reduce the formation of tertiary structures. MgOAc causes the reaction to start as soon as it is added to the mix. The tube was mixed by 6x inversions to start the reaction and briefly spun. Then the tube was placed in the Gentier 48E Real-time PCR System (Xi'an Tianlong Science and Technology Co., China) at 37°C with the lid switched off, for an amount of time between 15-60 min depending on the assay. Each assay was made in duplicates. For the detection of the product of amplification by LFA strip A, the protocol followed was the same as in Chapter 3.1 for the detection and the image processing. It is important to note that assays from RPA1.1 to RPA1.4 were made with strips A in the form of dipsticks (already cut as a strip) with an old lot that may possibly alter those results.

#### *2.5.1.1 RPA1.1*

For this assay, the amplification was carried out for 20 min. For the detection, the RPA product was 1:25 diluted and 10 µL of the dilution was applied with 80 µL of buffer B on the sample pad of strip A.

#### *2.5.1.2 RPA1.2*

This second assay differs from the previous one for the amplification time which lasts 60 min.

#### *2.5.1.3 RPA1.3*

This third assay has an amplification time of 15 min. For the detection of the RPA product by LFA, the total amount of RPA product (50 µL) was applied to the strip without dilution, with 40 µL of buffer B. The target concentration tested was $10^{10}$ copies/mL. Some controls were also done: a negative control with the same protocol but without the target DNA, one named “no oligonucleotides” without primers, probe and target DNA, one without primers and another without probe. All the elements removed from the mix were replaced by nuclease-free water. A positive control was also done. All controls were made in duplicate.

The positive control was supplied with the RPA kit and followed this protocol: in a 1.5 mL tube was mixed 8 µL of oligo mix with 25 µL of 2X reaction buffer. The mix was put in the vortex and briefly spun. Then 5 µL of 10X Probe E-mix was added with 0.9 µL of dNTP (100 µM) and 2.6 µL of nuclease-free water (to reach 3.5 µL). Then, 2.5 µL of the 20X Core reaction was added to the tube lid, mixed by 10x full inversions and briefly spun. 1 µL of the 50x Exo was added to the tube lid and mixed by 10x full inversions and briefly spun. The solution was transferred to a 0.2 mL PCR tube. 4 µL of 280mM MgOAc and 1 µL of positive control DNA were added to the tube lid, DNA and MgOAc should be kept separate in tube lids prior to spin-down. The tube was mixed by 6x inversions to start the reaction and briefly spun. Then the tube was placed in the fluorometer and followed the same protocol as the others.

#### *2.5.1.4 RPA1.4*

In this assay, half of the RPA product (25 µL) was applied to strip A with 65 µL of buffer B. The other half of the RPA product was analyzed on another strip to study the standard deviation of the strips for the same RPA product and compare the results with an assay where one tube was analyzed on one strip with two replicas.

#### *2.5.1.5 RPA1.5*

This assay is the same as the one before, except that one condition was done with another lot of strips, manually cut with a guillotine, the same lot as the one described in chapter 3.1.1, and another condition with the older lot of pre-cut strips previously used for the RPA assays, to study if the older lot had an impact on the assays.

#### *2.5.1.6 RPA1.6*

To be closer to the disc proportion of reagents described in chapter 3.2.2, an assay with the new strips cut from the uncut sheet was done with 8.5 µL of RPA product and 82 µL of buffer B with triplicates. Controls were done in the same conditions with the synthetic dsDNA mix, one NTC. Another assay was done in the same conditions but with the sample pad of the LFA strip cut with a blade, leaving 3 mm of sample pad for sample application.

### 2.5.2 RPA2

For this experiment, a similar protocol to RPA1.6 was used but with the Fw_primerPCR-RPA2, Rv_primerRPA2 and Probe_PCR-RPA2. For the LFA detection, a new lot of dipstick strips A was used (same as in chapter 3.2.2). Moreover, the buffer A that came with the new lot of strips A was used from now on for all the experiments until the end of this work. 5.7 µL of RPA product was applied on the sample pad with 109 µL of buffer A. The concentrations tested were $10^4$ and $10^5$ copies/mL and a blank, with duplicates each. The images were processed with the same method as in chapter 3.2.2.2.

### 2.5.3 RPA3

#### *2.5.3.1 RPA3.1*

This assay was conducted with Fw_primerRPA3 (23.8 µM), Fv_primerRPA3 (23.8 µM), Probe_PCR3-2 (83.3 µM), the TwistAmp® Liquid basic kit (TwistDx, UK) and an endonuclease IV (Nzytech, Portugal). It is important to note that the TwistAmp® nfo kit couldn't be used in this work because of its current commercial unavailability. First, a primer and probe solution was prepared in a 2 mL Eppendorf with 0.88 µL of Fw_primer, 0.88 µL of Rv_primer and 0.07 µL of probe. In a separate 2mL Eppendorf, the premaster mix solution contains 25 µL of Liquid Reaction Buffer 2x, 5 µL of Probe E-mix 10x, 3.6 µL of dNTPs (25 mM), 8.5 µL of water (to reach 12.1 µL), 2.5 µL of Core reaction mix 20x and 0.05 µL of Endonuclease IV. Then the primer and probe solution was quickly added to the pre-master mix solution and mixed. A PCR tube was placed on a frozen support for PCR tubes from Eppendorf and 46.5 µL of the previous solution was added to it. 2.5 µL of MgOAc and 1 µL of template cDNA were added to the tube lids in individual spots that don't touch as DNA and MgOAc should be kept separate in tube lids prior to spin-down. To finish the tube was spined and mixed by poking the Eppendorf with the finger. Then the tube was placed in the Gentier 96E Real-Time PCR System (Xi'an Tianlong Science and Technology Co., Ltd) (fluorometer) at 37°C, for 20 minutes. This assay tests concentrations ranging from $10^3$ to $10^{11}$ copies/mL with duplicates for each concentration.

For detection by LFA strip A, an image was captured of the strips at t0 by Leica DMS300 Digital Microscope System, and the strips were placed in lateral flow cassettes. Then 5 µL of RPA product was applied to the sample pad alongside 70 µL of buffer A. The results were captured after 15 min and the

images were processed with the software ImageJ (National Institutes of Health, USA) following the same method as in chapter 3.2.2.

For detection on disc with rotation, the protocol followed was the one from chapter 3.2.3, with 32 µL of RPA product and 109 µL of buffer A, with concentrations ranging from $10^3$ to $10^{11}$ copies/mL with two replicas per concentration and two NTC.

#### *2.5.3.2 RPA3.2*

##### 2.5.3.2.1 Amplification

This assay was conducted with Fw_primerRPA3 (23.8 µM), Fv_primerRPA3 (23.8 µM), Probe_PCR3-1 (83.3 µM) and the TwistAmp® Liquid exo kit (TwistDx, UK). First, a primer and probe solution was prepared in a 2 mL Eppendorf with 0.88 µL of Fw_primer, 0.88 µL of Rv_primer and 0.07 µL of probe. In a separate 2mL Eppendorf, the premaster mix solution contains 25 µL of Liquid Reaction Buffer 2x, 5 µL of Probe E-mix 10x, 3.6 µL of dNTPs (25 mM), 7.6 µL of water (to reach 11.2 µL), 2.5 µL of Core reaction mix 20x and 1 µL of Exo 50x. The remaining steps of the amplification protocol follow the same steps as in chapter 5.3.1. The concentrations tested range from $10^3$ to $10^{11}$ copies/mL with two replicas per concentration and two NTC.

##### 2.5.3.2.2 Amplification Product Detection

###### 2.5.3.2.2.1 Real-time detection on fluorometer

The fluorescence was measured on the Gentier 48E Real-time PCR System (Xi'an Tianlong Science and Technology Co., China), at 30s and then every 5 min until the end of the 20 min of the amplification. The evolution of the fluorescence at each point will then allow us to quantify the evolution of the amplification throughout the cycle.

###### 2.5.3.2.2.2 Detection by fluorescence microscopy

The microfluidic disc used is an existing one already developed and commercialized since October 2019 by the company biosurfit (Azambuja, Portugal) called the spinit® CRP disc. The entirety of the disc was not used for this assay, only the detection chambers (**Figure 21**). A fluorescence microscope built in-house (**Figure 22**), was used for signal detection regarding the previously performed amplification protocol. The blue laser beam goes through the mirrors that are here to guide the laser until the dichroic mirror. It then goes through the objective that contains two lenses and ends up reaching the disc chamber that contains the fluorescent analyte. The laser beam will excite the fluorophore contained in the sample (in this case, FAM) which will result in the emission of a signal that will reach the camera. A blue laser was chosen as its wavelength is within the excitation peak of FAM (λex 493 nm). Pictures were taken with the bright field (white light coming from under the disc) and with the blue

laser beam for comparison. The microscope was set up with the following conditions: exposure 1EV, shutter 66 ms, gain 24 dB and frame rate 15 fps.

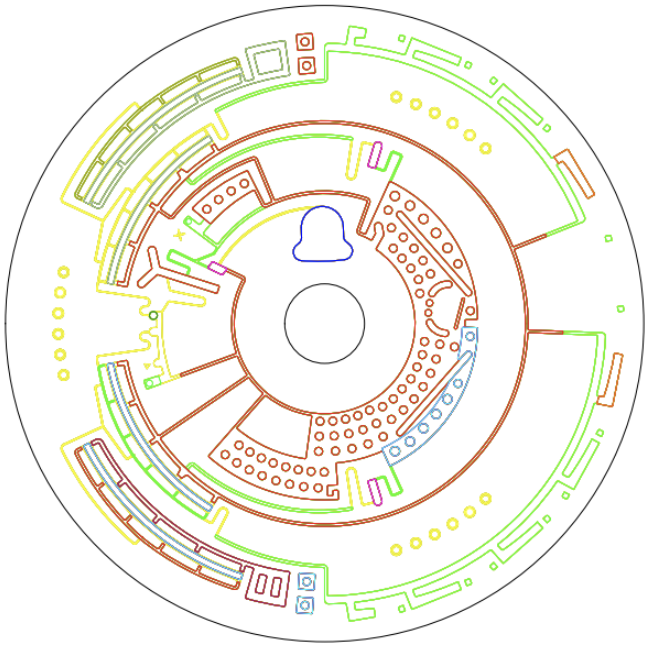

**Figure 21: Microfluidic layout from the CRP disc obtained from biosurfit**, detection chambers are located on the right side of the disc and highlighted in green (further explanation of the layout is available in the supplementary material).

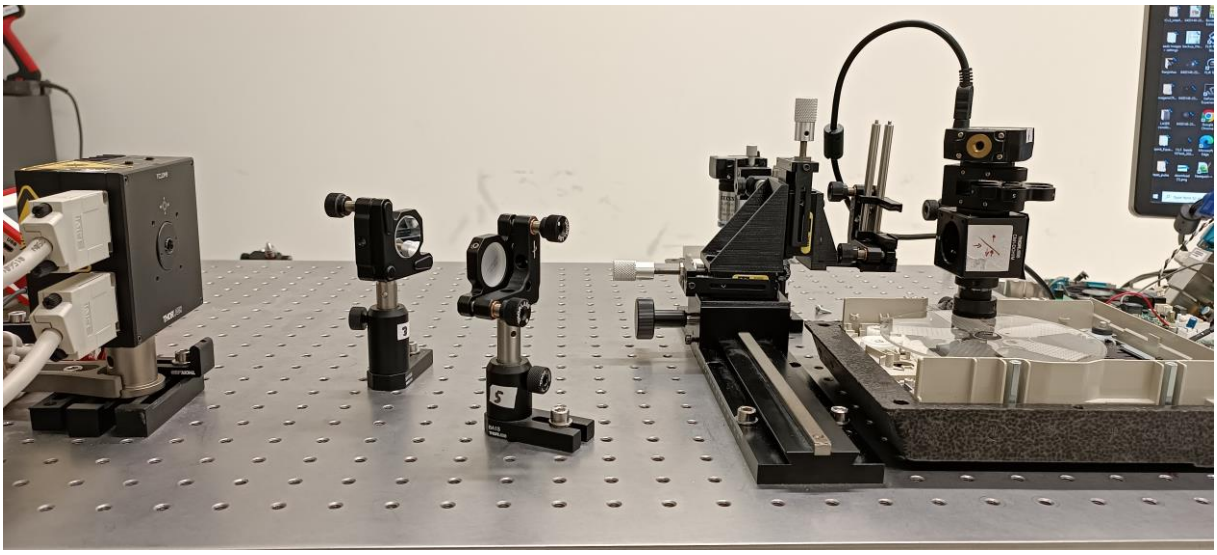

**Figure 22: Tabletop set-up of the fluorescence microscope prototype.**

# 3. RESULTS AND DISCUSSION

## 3.1 Validation of the strip for LFA

For nucleic acid detection, the selection was made between two different strip candidates: one containing AuNP (strip A) and the other CNP (strip B) (see **Chapter Introduction, Subchapter RPA-LFA (Lateral Flow Assay**)). Due to company policy, the exact denomination of the strips cannot be disclosed in this work. The strips were ordered in the form of uncut sheets and were cut manually in the production line of the company with a guillotine, with a width of 3.3 mm. To evaluate both strips and determine the one to be used in the following assays, the LoD was calculated. Based on the LoD, we selected the strip with the highest sensitivity. The LoD was obtained using a synthetic dsDNA mix of a known concentration that works as an analogue to a product of the amplification. The analysis of the different concentrations of synthetic dsDNA mix ranging from 0 to 1 nM gave mean grey values for the test line represented in **Figure 23.A**. Then a normalization of those values by dividing them by the mean grey values of the control line, following the method from Kaminski *et al.*, 2020 [93], was calculated and represented in **Figure 23.B**. However, those values don't seem to concord with the non-normalized ones as the shape of the curve drastically shifted and the values are not suitable for the calculation of the LoD. This result was expected as the LoD typically allows identification of the lowest point where the signal is distinguishable from the background noise, hence why it seems more appropriate to use the background signal as a normalization to give a better understanding of the noise level. This is what was done in **Figure 23.C** and allowed to show that the strip B based on CNP allows a LoD down the nanomolar range at 0.34 nM. The usage of the background signal as a normalization was the one that was decided to be followed for the study of strip A and showed that this strip based on AuNP allows a detection down to 0.06 nM (**Figure 24**). Therefore, strip A resulted in the highest sensitivity. Moreover, it is important to note that during the assays, strip B tended to shred once it was wet with the reagents, which consequently could affect the results. For those reasons, strip A was chosen to carry on the next assays.

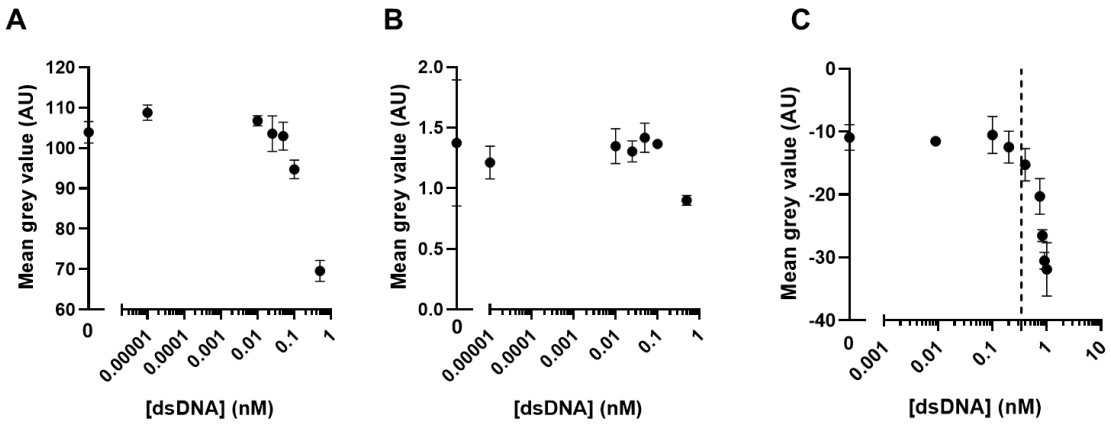


**Figure 23: LFA-based detection by strip B of the synthetic dsDNA mix (n=3).** Data are mean ± s.d. of three independent reactions. **A**: With mean grey value of the test line only **B**: normalized by dividing with the control line value **C**: normalized by subtracting with background value. LoD is symbolized by a vertical line.

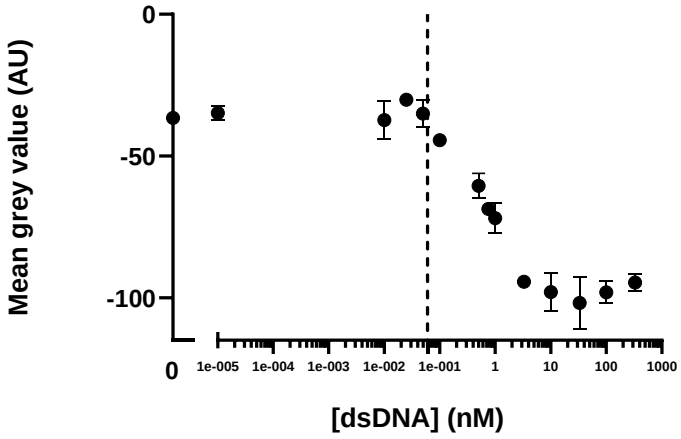


**Figure 24: LFA-based detection by strip A of the synthetic dsDNA mix (n=3).** Data are mean ± s.d. of three independent reactions and were normalized by subtracting with background value. LoD is symbolized by a vertical line. Concentrations are ranging from 0 to 330 nM.

## 3.2 Integration of the LFA in the microfluidic disc

### 3.2.1 dsDNA detection by direct dispense on LFA strip integrated on disc, without disc rotation

To minimize development time and costs, a decision was made to leverage a pre-existing microfluidic layout based on lateral flow previously developed by biosurfit. The disc layout used is the spinit® COVID-19 Antibody point-of-care blood test, which is a DVD-like disc that directly integrates the steps of sample preparation and blood separation, and requires 30 µL of sample volume (from capillary blood) giving the results in 20 min time. The disc displays a blister that contains the running buffer, a sample insertion chamber, a sample check to ensure that liquid is correctly circulated through the microfluidic layout during the rotation, and a chamber for the lateral flow strip. It also displays an S membrane right before the lateral flow strip, to ensure that the liquid can rightfully reach the membrane (**Figure 11**). As mentioned in chapter 3.2.1, the microfluidic disc was designed for the COVID-19 LFA, displaying a membrane chamber with a shorter length than strip A, which was chosen to carry on the

assay, hence why the absorption pad of strip A goes out of the chamber and interferes with the bonding of the tape that closes the disc (supplementary material **Figure 45**). The solution to this issue is to cut 1.2 cm of the strip. It is not advisable to cut the complete 1.2 cm in the sample pad as it contains the AuNP necessary for the detection, and after discussion with the R&D director of the company that supplies strip A, he recommended not cutting more than 0.7 cm of the sample pad. On the other hand, cutting too much on the absorption pad could also have a possible effect on the flow of the reagents through the strip and slow the time of the assay. Then, the choice was made to test two configurations: configuration A where 0.7 cm was cut on the sample pad and 0.5 cm was cut on the absorption pad, and configuration B where 1.2 cm was cut entirely on the absorption pad.

In addition, the other condition tested in this assay is the buffer used, since buffer A was now available (supplied with the strips A), while buffer B was the only one used for the assays until now. Buffer A is known to be a TBST (Tris-Buffered Saline with Tween-20) buffer, while buffer B's composition isn't disclosed by its supplier. It is important to note that the results disclosed in this section as well as the next ones cannot be compared to the previous chapter as the normalization of the current results isn't using the background signal anymore. Instead, it made more sense to quantify the background noise because the LoD typically allows identification of the lowest point where the signal is distinguishable from the background noise, so it would be more appropriate to take the value at t0 of the assay, at the same exact spots where the test and control lines would appear at the end of the assay (t15). This method also allows us to take into consideration the control line for normalization, which encloses more accurate results. Since this method involves a t0 capture of the results on the strip and those results were not measured for the previous experiments, the previous chapter follows a different analysis. For the t0 picture, it is expected to see a curve going up (**Figure 25**). For the t15 with a visible test line, two deeps in the curve should be visible. The one on the left corresponds to the test line and the one on the right to the control line of the strip.

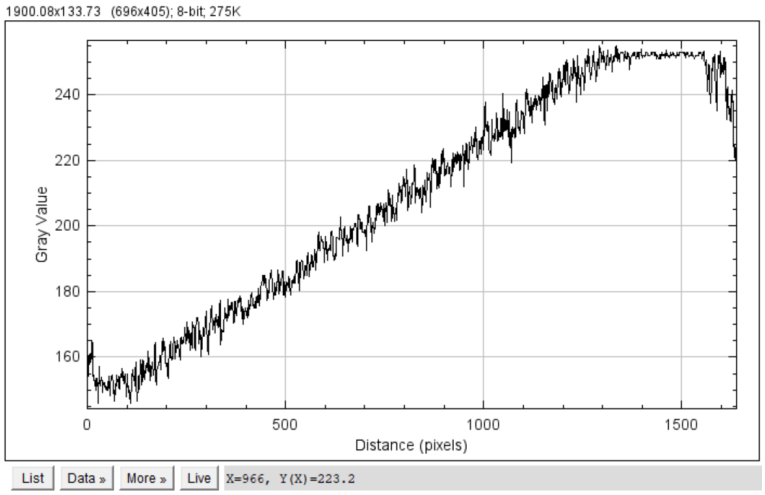


**Figure 25: Plot analysis at t0.**

The results are displayed in **Figure 26.A** and show very low ratio values for buffer B, which is linked to the lower intensity of the signal on the test line of the strip. Thus, buffer B was not indicated to pursue the next assays. Since the composition of buffer B is unknown, this result cannot be explained by its composition. However, buffer A was supplied with strip A, which is the one used for this assay, and the most compatible with strip A, from the buffers tested. Also, buffer A is a standard TBST buffer, that is particularly indicated for lateral flow assays [99] giving high ratio values for configuration A of the strip with buffer A but with a high variability of the assay, while configuration B shows lower ratio values with a smaller variability. In this case, the choice of the smaller variability was made, as it is more important in the development of the test to be able to have reproducible results while testing patients in the future.

To finish, the results from **Figure 26** are calculated by using the analysis with pictures at t0 and t15. **Figure 26.B** shows an extremely high variability of the ratios, indicating that normalization of the values shouldn't be proceeded by dividing the control value by the test value for the following assays, it is then preferable to normalize the ratio like in **Figure 26.A** by dividing the value of the test line by the control line, the same method reported by Kaminski *et al.*, 2020 [93] and Danthanarayana *et al.*, 2023 [100].

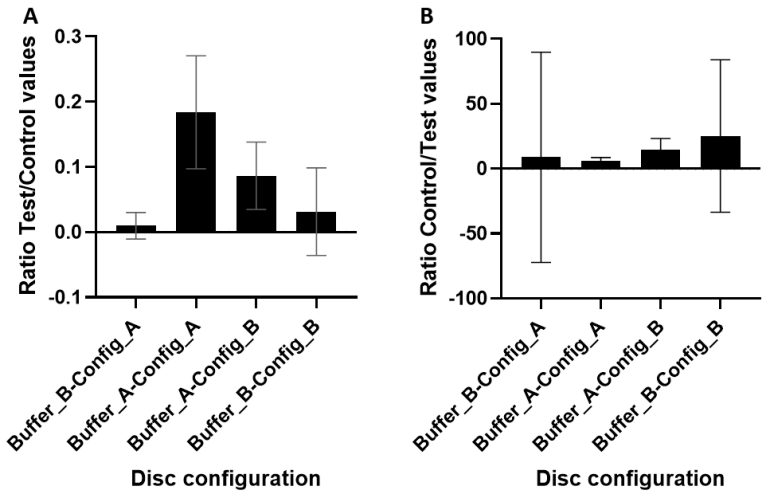


**Figure 26: Comparison of the buffer and strip configuration by synthetic dsDNA mix on the microfluidic cartridge (n=3). A**: With ratio made of test/control values. **B**: With ratio made of control/test values.

Since strip A, with the configuration B and buffer A was determined as the most suitable for the next assays, the previous assay was repeated for this condition, for concentrations of the synthetic dsDNA mix ranging from 0 to 150 nM. **Figure 27** shows a detection down the nanomolar range at 0.54 nM, which represents around $3.21 \times 10^{11}$ copies/mL. Those results show a higher value of LoD than on the assays outside of the disc that displayed a detection down to 0.06 nM, which is about $3.56 \times 10^{10}$ copies/mL. But as previously stated, the normalization of the values is different than in the previous chapter, also this assay takes place inside the disc, and even though the microfluidics were not used here, this assay undergoes a certain loss of the reagents while going first through the S membrane and then the LFA strip. Furthermore, the pressure exerted on the LFA strip by the tape that serves to close the disc can also contribute to an uneven dispersion of the reagents through the strip which leads to lower detection and/or higher variability.

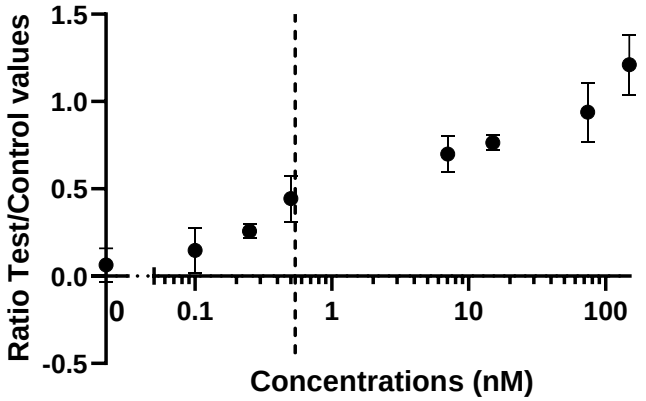


**Figure 27: The sensitivity of the LFA-based detection by strip A of the synthetic dsDNA mix by direct dispense on the microfluidic cartridge (n=3).** Data are mean ± s.d. of three independent reactions. LoD is symbolized by a vertical line.

### 3.2.2 dsDNA detection in LFA strip integrated on disc, using disc rotation for liquid control

Given the promising results that were obtained from the direct dispense on the disc, the assay was done with the synthetic dsDNA mix applied on the disc but with the use of the microfluidic layout and the rotational protocol. First, to be sure that the microfluidic layout operates as expected, a preliminary test was done using dyes, a blue dye to represent the synthetic dsDNA mix was placed in the sample chamber and a yellow dye was placed in the buffer chamber. The goal was to confirm that no abnormality was taking place during the assay, like a loss of liquid while making its way through the layout for example.

In **Figure 28** right, the blue dye (sample-like) reached the chamber of the S membrane (called S membrane due to the S shape of the chamber that contains a membrane) while leaving some of the dye in certain places in the microfluidic layout called “sample checks” that are here to ensure that the liquid rightfully went through the layout without any mistake. The same observations can be made for the yellow dye (buffer-like), which shows that the liquid went effectively through the microfluidics. The assay with the synthetic dsDNA mix can then be conducted with this disc.

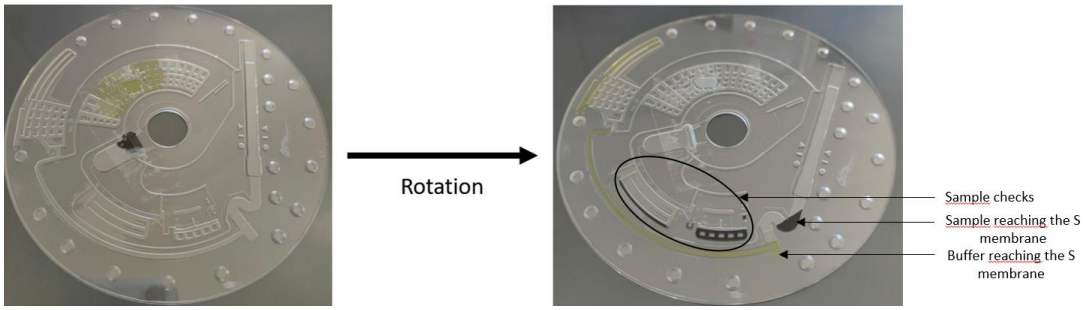


**Figure 28: COVID-19 disc**. Tested with the dyes applied in their respective chambers before rotation (left) and after rotation (right).

While injecting the buffer to conduct the assay with the synthetic dsDNA mix, it appeared that the buffer was overflowing due to the fact that the buffer was not distributed correctly through the chamber, to remediate this issue, a hole was made in the chamber with a blade, and the liquid was sucked through the hole to allow it to be distributed equally through the chamber as it illustrated in **Figure 29**.

**Figure 29: Suction of the buffer to distribute it through the chamber.**

Once this issue was resolved, concentrations of the synthetic dsDNA mix ranging from 0 to 20 nM were tested using the rotational protocol. **Figure 30** shows a geometric graph with detection down the nanomolar range at 2.52 nM, which corresponds to $1.53 \times 10^{12}$ copies/mL. Those results show a higher value of LoD than on the assays without the rotation (LoD =0.54 nM). For comparison from the literature, work with detection of DENV2 by RPA showed a detection down to $1.2 \times 10^{3}$ copies/mL [101], but this work used real-time detection of RPA and is not using a microfluidic platform for the test, which is the reason why a loss of detection is observed in this work compared to the literature. Once again, this loss of detection was expected as the assay is more similar to the final assay desired, with all the losses and possible interferences that come with the use of microfluidics. The use of microfluidics implies that a part of the reagents gets lost in the microfluidics and the entirety of the reagents displayed in the chambers do not reach the S membrane and then the LFA strip. This is explained by the fact that, as stated before, part of the reagents is stuck in some part of the microfluidics on purpose (sample and buffer checks) to ensure that the dispersion of the liquid during the rotation went well. But another element to take into consideration is that the theoretical calculations that were made by the engineers who designed the COVID-19 disc about the amount of reagents that reaches the membrane, was calculated especially for the original purpose of the disc which is COVID-19 detection. In this work, the disc is used for the purpose of Dengue detection which implies that the conditions are not the optimal ones. Alternatives would include a change of microfluidic disc, which was not possible during this thesis timeframe, as the design of a new disc would require more time and expenses but can be left for future improvements. Another alternative could be optimizing the proportions of the sample and buffer applied to the disc to help improve the assay.

Indeed, in practice, some differences can be seen during the assays. That is probably the case here, which would explain why there is a slight difference in the LoD for this assay. To overcome this issue, a future assay could include testing different proportions of sample and buffer, with gradually higher amount of sample and lower amount of buffer to try to see which proportions will allow a good balance with enough sample to allow a good detection with less variability but with enough buffer to allow the mix to flow through the LFA strip.

Despite this issue, a detection was still achieved with the synthetic dsDNA mix on the rotating disc while using the centrifugal microfluidic which leads us to the next step that is managing to move on to the amplification module, firstly by the gold standard PCR as a comparison method with the RPA assays that will then follow.

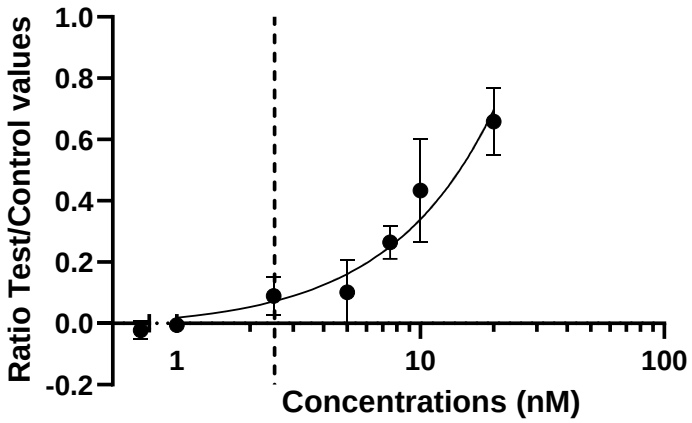


**Figure 30: The sensitivity of the LFA-based detection by strip A of the synthetic dsDNA mix on the microfluidic cartridge with rotational protocol (n=3).** Data are mean ± s.d. of three independent reactions. LoD is symbolized by a vertical line.

## 3.3 Validation of Real-time PCR (qPCR) and PCR protocol and primers for comparison with the RPA assay

### 3.3.1 PCR1

To test the first set of primers/probe PCR1, a PCR amplification was carried out with a detection by LFA strip A. Moreover, two different probes, Probe_PCR1 and Probe_RPA1, were tested to analyse which one was the most adequate for the detection by LFA. In theory, Probe_RPA1 should be the most adequate since it was specifically designed for post-amplification detection by LF, while Probe_PCR1 is more suitable for the detection of the product of amplification by gel electrophoresis after a conventional PCR. The results are displayed in **Figure 31**.**A** and agree with the expected result. Indeed, since the value mean grey value of the control line is divided by the background (those assays were made before the assays using the ratio test/control values), the normalized mean grey value should be smaller if the intensity of the test line is high. To sum up, the lower the mean grey value, the better the detection by LFA. In this case, Probe_RPA1 gives a lower value and a higher intensity when compared with

Probe_PCR1, which shows better detection. This observation is also confirmed by **Figure 31**.**B** and **C** that show a higher intensity of the test line for Probe_RPA1. These results confirm that this Probe is more adapted for LFA detection.

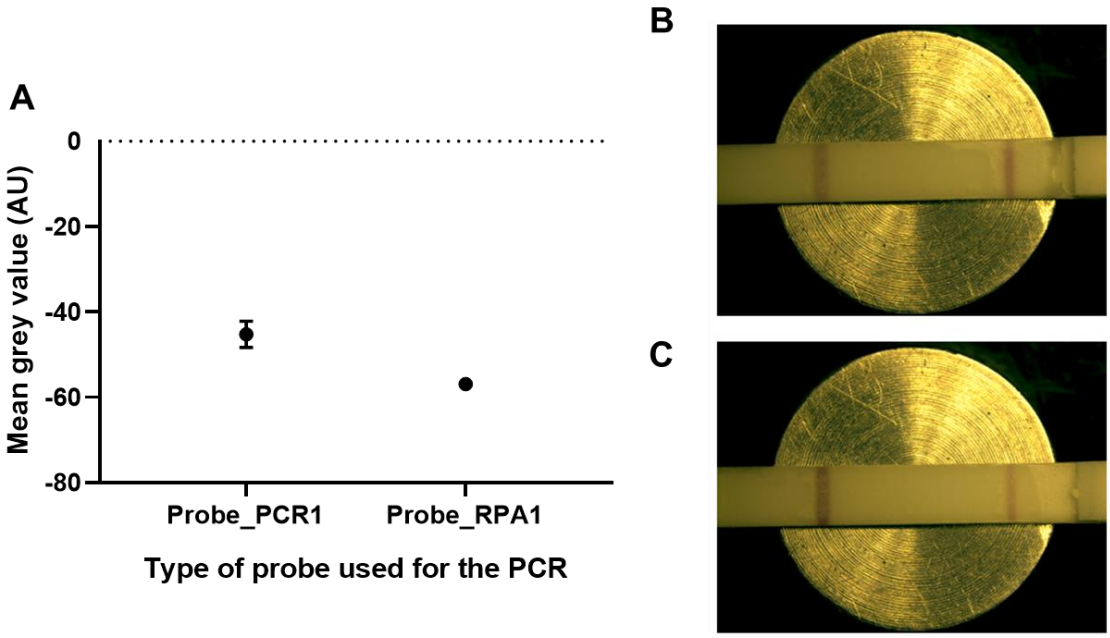


***Figure 31: LFA detection of the PCR1 at $10^{10}$ copies/mL (5.36 pM) of the target. A** : After quantification of the mean grey values (n=2), Data are mean ± s.d. of two independent reactions. **B**: Visual results with Probe_PCR, the left line is the test line while the right line is the control line **C**: Visual results with Probe_RPA, the left line is the test line while the right line is the control line.*

Complementary tests have been done by qPCR with Probe_qPCR1, however the real-time fluorescence could not be detected on the fluorometer. An assay was also done by PCR with detection by gel electrophoresis where the product was detected even in the NTC. The same assay was also done with shorter primers Fw_primerPCR-RPA2, Rv_primerPCR2, and Probe_PCR-RPA2 and the same results were seen in the gel (**Figure 47**, **Figure 49**). All those assays are detailed in the supplementary material. Since the NTC presented amplification, we conclude that probably primer-dimers were probably being formed with the conditions tested in this assay.

### 3.3.2 qPCR3-4

Different combinations of primers from the literature were tested[90], [91] for this qPCR assay, with the probe PCR_probe3-4. The visualization of the Ct values given by the fluorometer during the amplification that can be seen in **Figure 32.A**, shows that only three combinations of primers managed to give amplification and Ct values ≤ 29, which are strong positives: PCR3 (Ct=25.5), PCR3-4a (Ct=27.3) and PCR3-4b (Ct=27.1). The other pairs didn't give any amplification curve. Even though the PCR4 combination of primers is present in the literature, Fw_primerPCR4 doesn't align with the target sequence (**Figure 33**), consequently, this assay is not expected to give an amplification product. This assay is called PCR4.

Since the Ct levels are inversely proportional to the amount of target of nucleic acid in the sample, the combination of primers with the lowest Ct value gives the best amplification. In this case, the Ct values are very close to each other. The evaluation by agarose gel electrophoresis of these amplifications in **Figure 32.B** confirms that the size of the product of amplification is the one expected and as such, that the amplification was specific for the assays PCR3-4a and PCR3-4b with strong bands at 100 bp (which is the expected size of the amplicon), but shows a substantially faint band for the assay PCR3 at less than 100 bp (**Figure 33**). The gel also shows a product of amplification for the RPA3 assay at 100 bp, which wasn't displayed by the Ct values on the fluorometer. Overall, those results show that the assay PCR3-4 is the best combination of primers for the qPCR assays. Since the PCR3-4b (with 0.8 µM of primers) is the one displaying the lowest Ct value, between assays a and b, this combination is the one chosen as the best for the qPCR.

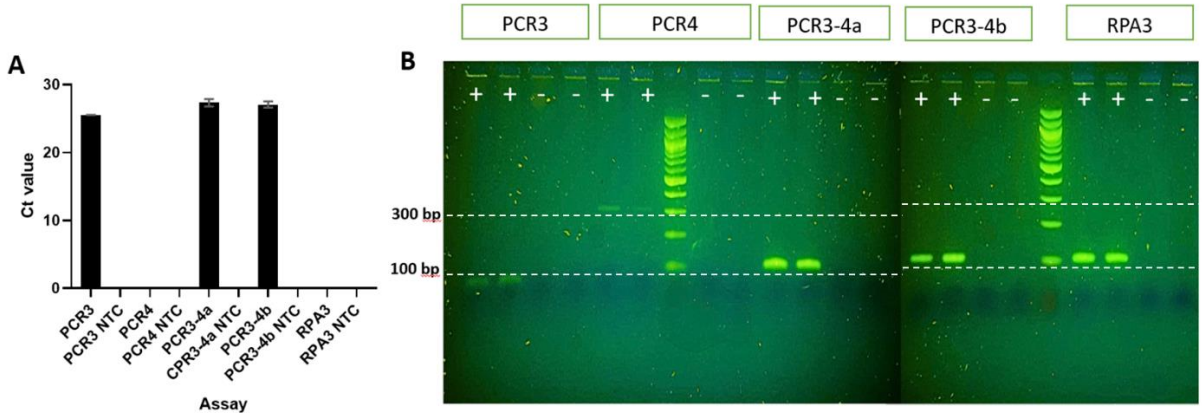


**Figure 32: Specificity of the PCR assay, depending on the combination of primers A**: Ct values obtained during the real-time amplification. Data are mean ± s.d. of two independent reactions. **B**: Detection of the product of amplification of the qPCR assay by 2.5% agarose gel electrophoresis with PCR3: Fw_primerPCR3 + Rv_primerPCR3 at 1 µM, PCR4: Fw_primerPCR4 + Rv_primerPCR4 at 1 µM, PCR3-4a: Fw_primerPCR3 + Rv_primerPCR4 at 1µM, PCR3-4b: Fw_primerPCR3 + Rv_primerPCR4 at 0.8µM and RPA3: Fw_primerRPA3 + Rv_primerRPA3 at 1 µM.

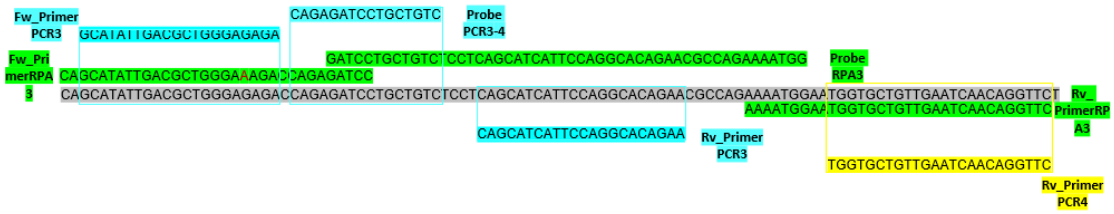


**Figure 33: Alignment of the sequences for PCR3, PCR4, PCR3-4 and RPA3 experiments.**

The efficiency of the amplification with the PCR3-4b primers (0.8 µM) was studied in **Figure 34** where each dot represents the mean Ct value from two replicates and the line represents the linear-log regression. This assay could distinguish differences in concentrations of a range from $10^4$ to $10^{10}$ copies/mL of target cDNA. The value representing the efficiency of the amplification is 109% ($R^2$=0.997; Slope =-3.114). Since the value showing a good efficiency of PCR amplification is within the range of 90-110%, it shows that those primers at 0.8 µM allow a good efficiency of the amplification.

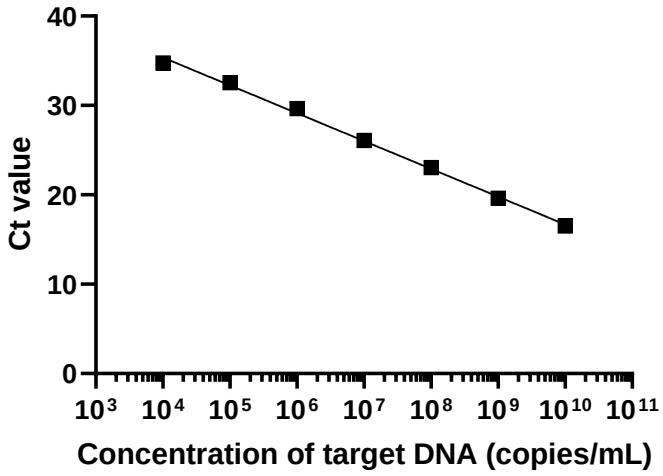


**Figure 34: Sensitivity of the qPCR assay using the primers PCR3-4a at 1 µM, with duplicates of tenfold serial dilutions of the target cDNA.**

## 3.4 RPA amplification and detection of the RPA product

### 3.4.1 RPA1

Amplification of the cDNA target ($10^{10}$ copies/mL) with Fw_primerPCR-RPA1, Rv_primerRPA1 and probe_RPA1 was made with two replicates and with detection by LFA strip A. The goal here is to determine the best duration of amplification between 20 min and 60 min. As represented in **Figure 35**, the mean grey values of the 20- and 60-min RPAs are slightly lower than the NTCs, but with a high variability that doesn't allow us to say that an amplification took place. Indeed, since the mean grey value is normalized by the grey value of the test line subtracted by the grey value of the background, it means that the lowest mean grey value corresponds to a higher intensity on the LFA strip, which is correlated with a higher amount of nucleic acid. The difference between the NTCs and the 20- and 60-min samples is not that significant and shows that these parameters are not optimal for this assay. The duration of the amplification might be one parameter to change, but also the fact that a 1:25 dilution of the RPA product was made before being applied to the LFA strip can contribute to those results. Those are the two parameters that were changed for the next assay.

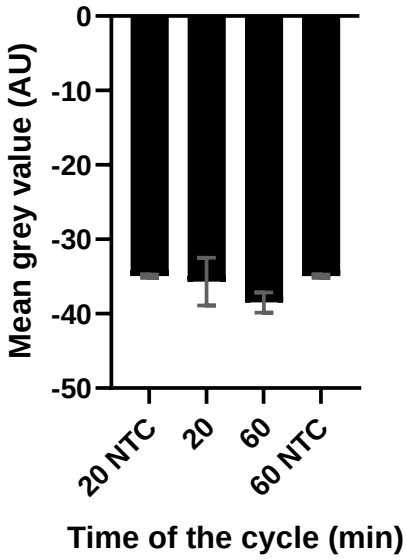


**Figure 35: LFA detection of the RPA with 20- and 60-min cycles.** Data are mean ± s.d. of two independent reactions.

The same assay was run but with a 15-minute cycle this time and the total amount of RPA product was used on the LFA strip, alongside a positive control and negative controls that include one without target DNA, one without primers, probe and target, one without primers and one without the probe and are all displayed in **Figure 36**. The $10^{10}$ copies/mL target assay gave a mean grey value 1.4-fold lower than the negative control (correlated to a high intensity of the test line and a higher amount of nucleic acid) but doesn't allow a detection as strong as the positive control, the latter being 1.2-fold higher. Moreover, the assay has a high variability and showed a result very close to the negative controls. The goal now will be to study how to reduce the high variability of this assay.

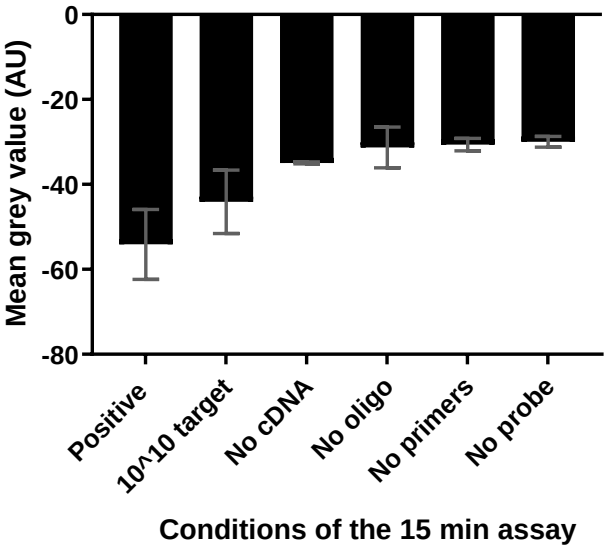


**Figure 36: LFA detection after 15 min RPA cycle.** Data are mean ± s.d. of two independent reactions.

The two elements that can contribute to the variability of the assay are either the RPA reaction itself with variability between each duplicate, or the detection module with the LFA strip. Since duplicates of the RPA reactions were done for all the previous assays, one way to study the variability is to use only half of the RPA product (25 µL) of each duplicate for detection on an LFA strip A each, and to compare with one RPA reaction that was separated in two with each half of the vial detected on one LFA strip A each, with all assays containing the same RPA mixture with $10^{10}$ copies/mL of target. The results are displayed in **Figure 37**.**A**, where it is shown that even with only one RPA reaction, even though the standard deviation of the assay is slightly reduced, it remains very high with a standard deviation only 0.7-fold lower than for the assay with two RPA reactions. This contributes to the hypothesis that the variability might come from the LFA strip itself. Moreover, during the assays, when one of the replicas was giving results close to the NTC, it became apparent that the gold nanoparticles tended to accumulate on the edges of the strip instead of flowing uniformly throughout the strip from the sample pad to the absorbent pad.

Furthermore, the strips used for the RPA detection can also present a loss of sensitivity over time once the box is open, or along the lot, which could have increased the results variability. For comparison, an uncut sheet supplied by the company from strip A was ordered and cut with a guillotine in the production line of biosurfit. According to the supplier, those two forms of the strips are supposed to be identical. It can be seen in **Figure 37**.**B** that the strip cut from the uncut sheet detects a higher amount of nucleic acid than the pre-cut ones (used previously in this work) from the same RPA reaction. Those results show a better detection from those new uncut sheets. From now on, the RPA assays were conducted with the strips cut from the uncut sheets.

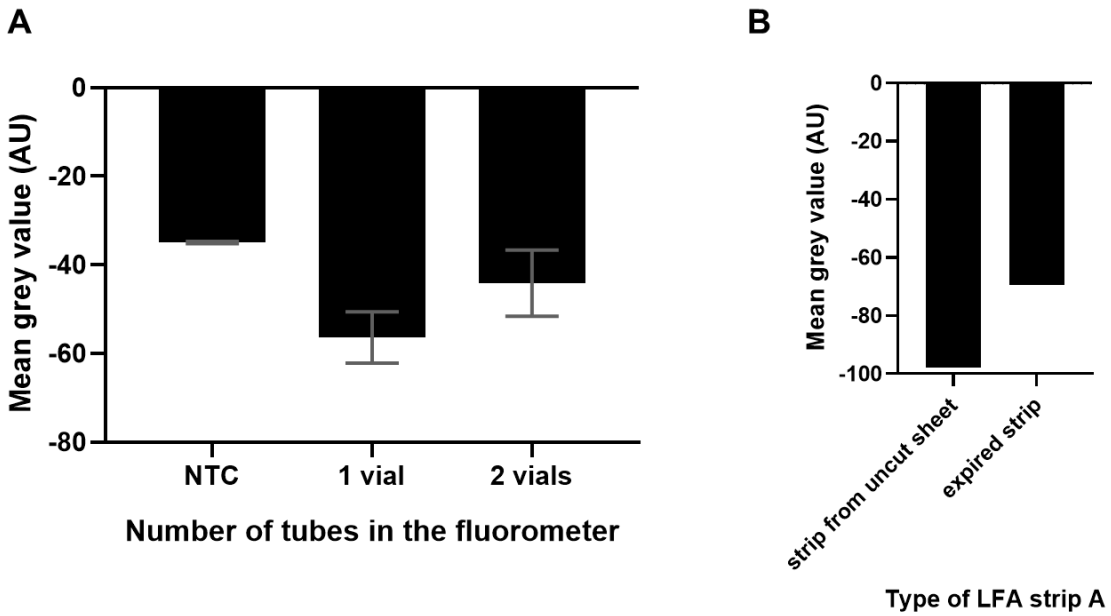


**Figure 37: Optimization of the variability of the RPA assay. A**: Study of the variability of the RPA reaction. Assay with half of an RPA vial detected on one LFA strip and the other half detected on another strip, compared to duplicates of half an RPA vial detected on one LFA strip (two independent reactions). **B**: Study of the variability of the strips cut with the guillotine from the uncut sheet versus the ones already cut by the supplier (previously used in this work). Data are from one independent reaction.

Despite the high variability of assays, better detection of the RPA product was reached with those new strips from the uncut sheets. The next step was then to try to have a detection with an amount of RPA product that is closer to the proportions from the COVID-19 disc which can be seen in **Figure 38** where 8.5 µL of RPA product was used with 82 µL of buffer B. The assay gave a comparable variability to the previous assay with 25 µL (25+65) but a higher amount of nucleic acid was detected. This can be explained by the fact that more running buffer was used for this assay, which could have contributed to a better mobility of the RPA product through the LFA strip during the detection.

Those results were then compared to a similar assay using the synthetic dsDNA mix, which showed a very good detection with a reduced variability of 30%, which can indicate that most of the variability observed in the previous assays was coming from the amplification rather than the new LFA strip itself. This was expected since the previous high variability observed coming from the strip was corrected by using those new strips from the uncut sheet rather than the pre-cut strips.

The next step for the LFA strip to be fully adapted to the disc is to be shortened to fit the dimensions of the chamber allocated to the LFA in the disc. The same proportions were used for this assay, but with a cut on the sample pad leaving 3 mm of sample pad for sample application. The mean grey value obtained for this assay is like the assay without the cut, so the cut of the sample pad doesn't have a considerable impact on the detection.

Since the RPA amplification seems to be the issue here, it seems like the set of primers/probes used for RPA1 might not fit the amplification and it would be necessary to design a more appropriate set.

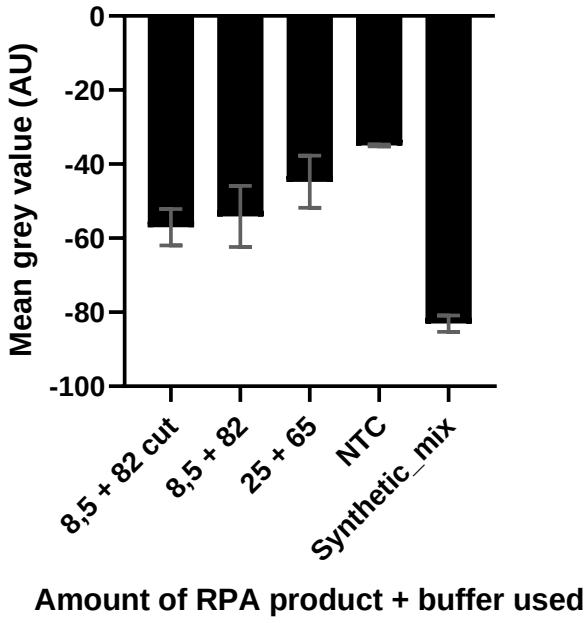


**Figure 38: Optimization of the future integration of the LFA strip in the disc.** Data are mean ± s.d. of two independent reactions.

### 3.4.2 RPA2

In order to optimize the previous assays, key elements were improved, such as new primers and probes sequences. The major improvement is the use of shorter sequences of primers and probes, that are highly recommended for PCR. Indeed, since longer sequences which are more advised for RPA reactions were tested in chapter 4.1, the new strategy in this chapter is to use sequences optimized for PCR assays (since the same sets of primers are used for both PCR and RPA). Then, to end any uncertainty about the LFA strips, a new lot was ordered in the form of dipsticks, which means that they were pre-cut by the supplier, which is more reliable and does not suffer from a possible loss of sensitivity over time as they are freshly ordered. In addition, the buffer previously used for the RPA assays was the buffer B supplied with the strips B because the buffer supplied with the strips A was past the expiration date and no buffer was supplied with the uncut sheets of strip A. That's why for this assay, buffer A that was supplied with those newly ordered strips A was used. Moreover, the proportions of the RPA product used were reduced to 5.7 µL (compared to 8.5 µL before) as it is exactly the theoretical amount of sample that reaches the S membrane in the disc after the use of the microfluidics, which will facilitate the integration in the disc if the assay is concluding. The amount of buffer was also optimized to 109 µL, as it was observed during the previous assays that the reagents had trouble going through the LFA strip.

Despite all the possible improvements made, the results displayed in **Figure 39** show once again very inconsistent values and variability of the assay and compared to the results that the PCR with gel electrophoresis gave with the same primers (supplementary material) that detected nucleic acid product in the blanks, it might be the same event occurring in this RPA assay, with the amplicon detected not being a product of amplification but either the result of contamination or the formation of primer dimers.

Since all the reagents were freshly opened right before the PCR assay, the primer dimer formation is the most likely scenario that took place. In conclusion, those primers are still not the optimal ones for this assay.

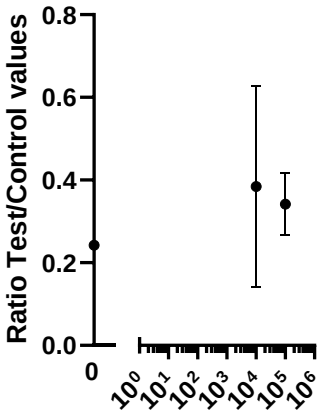


**Figure 39: Detection after RPA2 with shorter primers.** Data are mean ± s.d. of two independent reactions.

## 3.4.3 RPA3

### *3.4.3.1 Colorimetric detection*

Lastly, for these assays, the primers Fw_primerRPA3 (23.8 µM), Fv_primerRPA3 (23.8 µM), Probe_PCR3-2 (83.3 µM) found in the literature were used as their efficiency for RPA assays have been proven with a detection limit between $10^3$-$10^4$ copies/mL [89]. Since positive results were obtained in the PCR assays described in section 3.2, the primers were tested for RPA with detection on the LFA strip A. They were first tested at $10^4$ and $10^5$ copies/mL in **Figure 40.A** where the mean grey values are considerably higher (5.2- and 39-fold higher respectively for $10^4$ and $10^5$ copies/mL of target) than for the NTC (negative control). Since those primers were able to give a good amplification with RPA, a calibration curve was subsequently done to determine the sensitivity of the assay. The results can be seen in **Figure 40**.**B**, in which a positive result was obtained for the NTC. Since the conditions of the assay are the same as in **Figure 40.A**, the most likely reason for this is that a contamination must have occurred during assay B. Therefore, these results are probably not reliable, especially since in both figures, an assay was done at $10^4$ copies/mL and gave different mean grey values (0.1 for figure A and 0.4 for figure B) with a high variation for the assay displayed in figure B. However, in the assay displayed in **Figure 40.A**, a detection was reached for a target concentration of $10^4$ copies/mL, which is in accordance with the LoD from the literature. Further assays would need to be done to troubleshoot the results obtained in **Figure 40.B**, to be able to properly display a calibration curve that would allow to calculate a LoD.

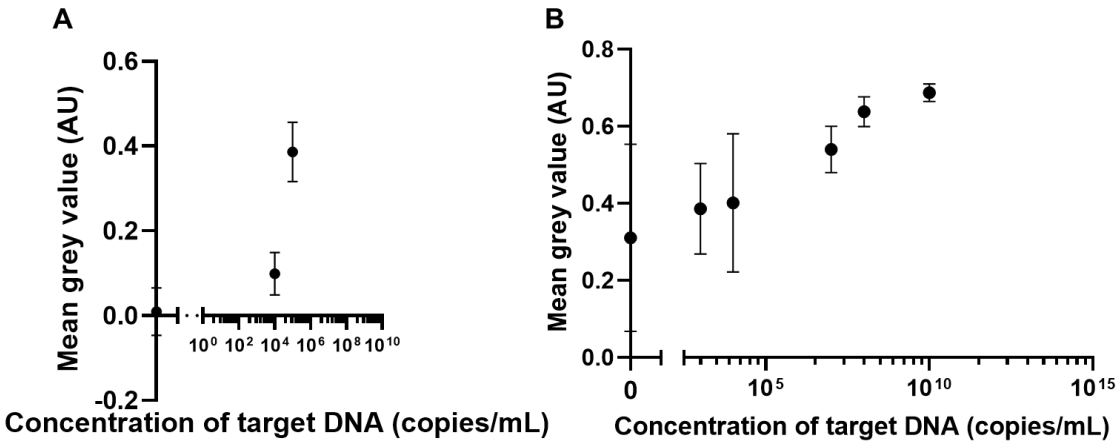


**Figure 40: RPA3 assay with detection on LFA strip A (on cassette).** Data are mean ± s.d. of two independent reactions.

To finish, a detection on the disc while using the rotation protocol was carried out and the results are displayed in **Figure 41**. Once again, the results showed very high variations and the NTC still gave a test line showing that a small amount of nucleic acid was detected. The latter might confirm the hypothesis from the previous assay, that one of the reagents might be contaminated. Moreover, the data from this curve have higher variations than the results from the assay on the cassette, which was slightly expected since the integration in the disc has more factors that could contribute to the variability since the reagents are going through the microfluidic layout of the disc and the S membrane. However, some improvements could be made as the current microfluidics were not specifically designed for this assay but for the COVID-19 disc, and the same can be said about the rotation protocol. The latter was already slightly improved before this assay as some samples were tested with the rotation protocol from the COVID-19 disc and the reagents had trouble reaching the LFA strip, which led to a new protocol used in this assay. However, with more time the protocol could be even further improved to fit the needs of the assay and allow better detection and standard variation of the results. The disc could also use some improvement, as a tailor-made disc for this assay would allow optimal conditions to have a proper and reliable detection. Those results are encouraging showing that a detection by LFA strip A while using the microfluidic disc is possible, but those elements from the disc, the protocol and the possible contamination would need to be studied in the future.

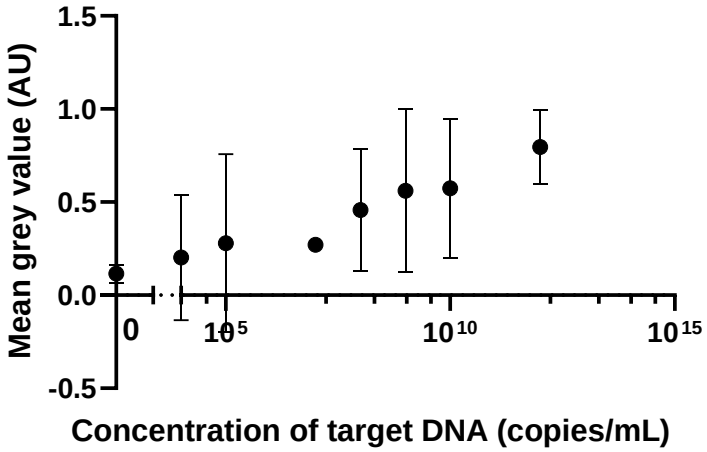


**Figure 41: RPA3 assay after rotation on disc with detection on LFA strip A.** Data are mean ± s.d. of two independent reactions.

### *3.4.3.2 Detection in bulk*

The LFA detection presented itself as a possible method for qualitative detection. However, to go towards quantitative detection, the use of fluorescence labels was studied. The in-bulk fluorescence detection was studied using biosurfit CRP disc. In the first approach, this implied carrying the amplification outside of the disc, then injecting the product of amplification into the detection chamber of the CRP disc and detecting it by a table-top prototype of a fluorescence microscope. Firstly, this assay was done with the usual synthetic dsDNA mix to see if this detection could be possible, which is shown in **Figure 42**. The results show an increasing fluorescence intensity when the quantity of target DNA increases. Then, the optimized RPA assay for fluorescence detection was carried out, but with the detection on the CRP disc chamber instead of the fluorometer.

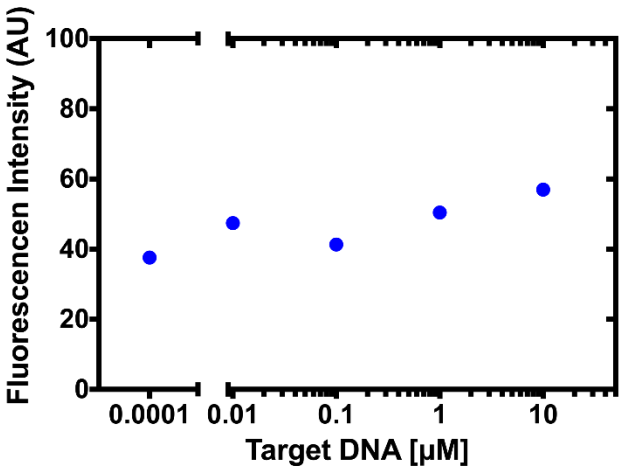


**Figure 42: Fluorescence detection by microscopy on the CRP disc chamber with the synthetic dsDNA mix (n=1).**

The detection in the CRP disc chambers of the RPA assay by fluorescence detection is displayed in **Figure 43.A** where once again, some fluorescence was detected in the NTC, which in accordance with the previous results of the RPA assays, could be either due to a contamination of one of the reagents or due to the fact that RPA can sometimes give false positives as this technique works very well at room temperature. However, samples containing the target cDNA show higher fluorescence levels than the NTC. Also, since the RPA reaction was carried outside of the disc, and then the RPA product was applied on the disc for detection, this could trigger more variability of the assay, as the samples had to be frozen to end the RPA reaction and then applied to the disc. Then, while placing the disc under the microscope, the time taken to find the right chamber and angle for the capture of the fluorescence with the laser, has a considerable impact on the levels of fluorescence, as the latter decreases when exposed for too long under the blue laser.

Moreover, as displayed in **Figure 43.B**, a considerable difference can be seen between the samples at $10^{10}$ copies/mL, the NTC, and the assay with only $H_2O$. Indeed, the NTC contains some white stains due to some noise from the disc, probably during the closing of the disc where some residual dust must have been intercalated while putting the closing tape. However, a clear fluorescence can be seen in the sample at $10^{10}$ copies/mL, showing that with optimization, a detection by fluorescence microscopy in the Spinit instrument is a possibility for the detection of DENV. In the literature, RPA rapid testing showed results with a detection limit down to $1.2 \times 10^4$ copies/mL for DENV2 [101]. Reaching that detection is the goal for future work.

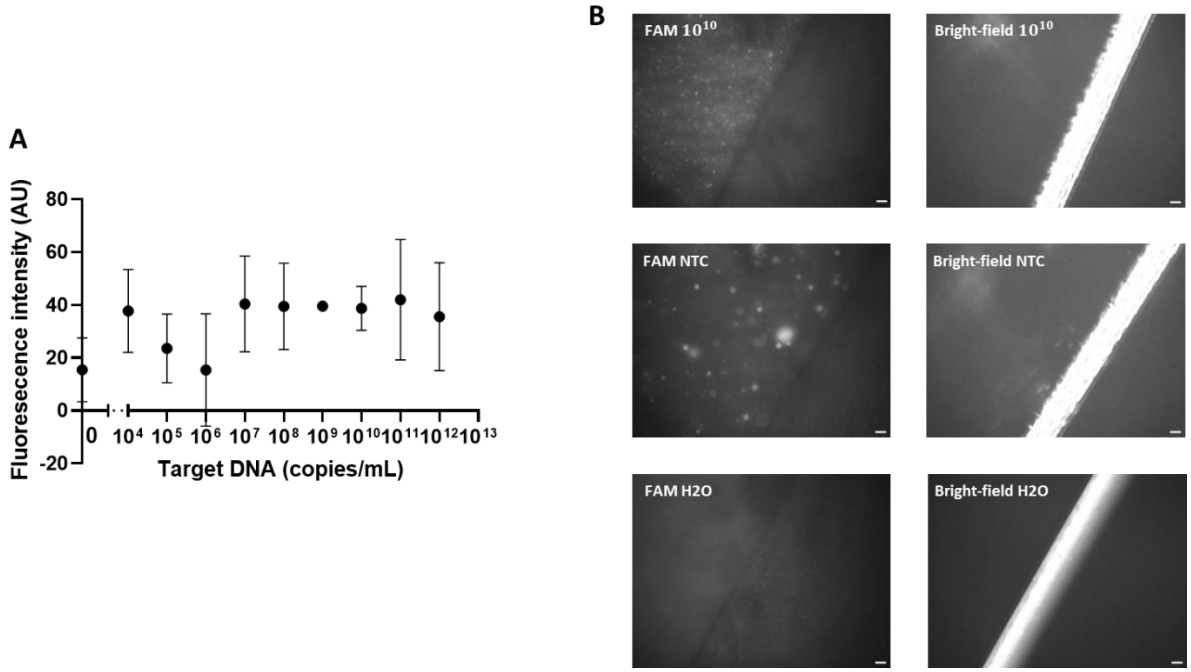


**Figure 43: RPA3 detection on CRP disc by fluorescence microscopy**. **A**: Sensitivity of the assay with concentrations of cDNA ranging from 0 to $10^{12}$ copies/mL. Data are mean ± s.d. of two independent reactions. **B**: Frame at the limit between the detection chamber (left side of each frame) and the rest of the disc without any reagents (right side of each frame). The frames labelled FAM are the ones taken under the fluorescence channel and the ones labelled "Bright-field" were taken under the white light.

# 4. CONCLUSION AND FUTURE PERSPECTIVES

This proof-of-concept study allowed the development of an *in vitro* diagnostic test for Dengue virus by the mean of a microfluidic platform with an isothermal nucleic acid amplification and a detection by LFA strip or in-bulk fluorescence. The most effective detection by LFA was chosen between CNP and AuNP, the latter allowing lower concentration detection was chosen to be integrated into the existing disc (called COVID-19 disc). This integration raised an issue as the LFA strip did not fit the chamber provided for this purpose in the disc. The choice was then made to cut the LFA strip on the absorption side, as cutting on the sample pad would imply a cut on the zone containing the AuNP and would have impacted the detection and its variability. Further in the integration in the disc, the buffer used in the assays was first buffer B but as assays went on, a new buffer called buffer A which is provided with LFA strips A, was found more appropriate for the assays. According to the supplier, buffer A is a standard TBST buffer, which is easy to be "homemade" prepared in the laboratory, and is the next step for further work to test and compare with the current buffer A. If the "homemade" TBST buffer was able to give good results, this could potentially reduce the costs of production of this *in vitro* diagnostic test, as buying directly the raw materials is usually financially advantageous. To finish the integration, the rotation protocol was tested with the synthetic dsDNA mix and showed promising results with a detection down to 2.52 nM, even though the amount of reagents reaching the membranes were not the ones that were theoretically supposed to reach it. It is expected in the field of microfluidics but opens the door to some microfluidic improvements of the disc to design a disc more adapted to this use for DENV detection, or for the design of a totally new microfluidic disc especially designed for this purpose.

In parallel, the normalization of the quantification of the signal from the LFA strip was improved, from starting from the value of the test line divided by the control line just like in the literature but was improved by dividing by the value of the background. Since those methods were still not rightfully reflecting the reality that can be observed by the eye, and that using the background or the control line for normalization had to each their own good, the method was improved and led to the final normalization displayed in 3.2.2.2 that is using both of those elements to have a more accurate normalization of the values.

On the amplification methodology work front, the RPA technique was compared to the gold standard PCR. For this purpose, different sets of primers were tested with both methods of amplification while respecting the design rules for each assay. The first set of primers didn't give conclusive results and showed DNA product in the NTC samples when detected by agarose gel electrophoresis after PCR which was the result of primer dimer formation. That is why a second set of shorter primers were then tested as they might be better suited to RPA and had less chances of primer dimer formation. Unfortunately, those primers still show a product in the NTC samples. Lastly, different combinations of primers/probe issued from the literature that showed consistent results were used and all tested for qPCR, PCR combined with agarose gel electrophoresis, RPA with lateral flow detection and RPA combined with fluorescence microscopy detection. The qPCR and PCR assay showed very good amplification, while the RPA assays gave more mixed results that are probably due in this case to a

contamination as the first RPA assay was at first giving good results. Unfortunately, due to time limitations, this couldn't be further investigated. This could be left for future work where the current reagents could be tested again to confirm this, and additional RPA assays could be run while changing one reagent each time to determine which one could be faulty.

The sensitivity achieved with the synthetic dsDNA mix is within the range of what can be found in the literature in terms of limit of analytical performance for a proper diagnostic of the presence of the disease, as we achieved a limit of 2.52 nM, which corresponds to $1.53 \times 10^{12}$ copies/mL and an RT-PCR test in the literature was found to achieve 357 copies/mL [102], which was 12-fold lower than the one achieved in this thesis, reinforcing that we could improve the results obtained. Moreover, another possible element to take into consideration for those results is the possible effect of the change of pH during the reaction of RPA, on the assay. A step for the future would be to study the effect of the variation of pH with a pH meter during the assay. Another possible method that wouldn't affect the assay is the Next generation sequencing.

Since this work was focused on showing a proof-of-concept of the possibility of developing this point-of-care test using this microfluidic platform, the goal can be considered reached as the microfluidic platform displayed acceptable performance regarding the detection of the synthetic dsDNA mix. Now, to pass from the proof-of-concept phase to a further one, a proper microfluidic platform specifically designed for this purpose would be optimal, as the optimal amount of buffer and sample for RPA are not the ones reaching the end of the current microfluidic disc and the needs to cut the LFA strip has a considerable impact on the detection of the amplification product. The development of a tailormade LFA strip could also be a possibility to be specific to the assay and have a strip of the exact dimensions that are needed. Regarding fluorescence microscopy detection, since a table-top fluorescence microscope prototype was used for detection, a comparison study of the detection could be done with a proper fluorescence microscope. Moreover, the development of a microfluidic platform that would allow the amplification, mixing steps and detection by fluorescence microscopy could also improve the results as in those assays, the RPA was carried outside of the disc and directly injected in the detection chamber. Regarding the amplification, further assays would be needed to optimize the RPA and comparison with other isothermal amplification techniques would be interesting to study. Also, using a purification column to purify the RPA product can allow for to detection of the product by agarose gel electrophoresis just like in Wang *et al.*, 2022 [103], which could possibly allow more information on the amplification, and to be able to compare with the results from the gel electrophoresis. Moreover, the final goal of this project is to multiplex the POC test to CHIKV and ZIKV, which is left for future developments. To finalize the project, instead of having cDNA as a starting material, to directly start from the extracted RNA of the virus and performing the step of reverse-transcriptase (as it was not the main goal of the project, the focus wasn't drawn to this step) and eventually, to start with biological samples of the virus, a step that couldn't be performed in the company biosurfit as it doesn't possess the safety equipment to work with viruses, but in partnership with an institute that has all the safety equipment like IHMT (Instituto de Higiene e Medicina Tropical), for example.

# 5. REFERENCES


[1] P. B. Deroco, D. Wachholz Junior, and L. T. Kubota, “Recent advances in point-of-care biosensors for the diagnosis of neglected tropical diseases,” *Sens Actuators B Chem*, vol. 349, p. 130821, Dec. 2021, doi: 10.1016/J.SNB.2021.130821.

[2] A. Zumla and A. Ustianowski, “Tropical Diseases: Definition, Geographic Distribution, Transmission, and Classification,” *Infect Dis Clin North Am*, vol. 26, no. 2, p. 195, Jun. 2012, doi: 10.1016/J.IDC.2012.02.007.

[3] P. J. Hotezid, S. Aksoyid, P. J. Brindleyid, and S. Kamhawiid, “What constitutes a neglected tropical disease?”, doi: 10.1371/journal.pntd.0008001.

[4] “World health statistics 2022: monitoring health for the SDGs, sustainable development goals.” Accessed: Feb. 08, 2023. [Online]. Available: https://www.who.int/publications/i/item/9789240051157

[5] L. E. Davis, J. D. Beckham, and K. L. Tyler, “North American encephalitic arboviruses,” *Neurol Clin*, vol. 26, no. 3, p. 727, Aug. 2008, doi: 10.1016/J.NCL.2008.03.012.

[6] D. Fischer, P. Moeller, S. M. Thomas, T. J. Naucke, and C. Beierkuhnlein, “Combining climatic projections and dispersal ability: A method for estimating the responses of sandfly vector species to climate change,” *PLoS Negl Trop Dis*, vol. 5, no. 11, Nov. 2011, doi: 10.1371/JOURNAL.PNTD.0001407.

[7] M. Wasay, I. A. Khatri, and F. Abd-Allah, “Arbovirus infections of the nervous system: Current trends and future threats,” *Neurology*, vol. 84, no. 4, pp. 421–423, 2015, doi: 10.1212/WNL.0000000000001177.

[8] M. Jie Alvin Tan Genome, M. L. Hibberd Genome, and N. Furnham, “Emerging Diseases,” 2017, Accessed: Oct. 14, 2023. [Online]. Available: http://portlandpress.com/biochemist/article-pdf/39/3/18/852069/bio039030018.pdf

[9] M. J. Sabir, N. B. S. Al-Saud, and S. M. Hassan, “Dengue and human health: A global scenario of its occurrence, diagnosis and therapeutics,” *Saudi J Biol Sci*, vol. 28, no. 9, p. 5074, Sep. 2021, doi: 10.1016/J.SJBS.2021.05.023.

[10] “Dengue and severe dengue.” Accessed: Feb. 08, 2023. [Online]. Available: https://www.who.int/news-room/fact-sheets/detail/dengue-and-severe-dengue

[11] “Dengue worldwide overview.” Accessed: Feb. 08, 2023. [Online]. Available: https://www.ecdc.europa.eu/en/dengue-monthly

[12] E. Gould, J. Pettersson, S. Higgs, R. Charrel, and X. de Lamballerie, “Emerging arboviruses: Why today?,” *One Health*, vol. 4, p. 1, Dec. 2017, doi: 10.1016/J.ONEHLT.2017.06.001.

[13] S. N. Slavov *et al.*, “Dengue seroprevalence among asymptomatic blood donors during an epidemic outbreak in Central-West Brazil,” *PLoS One*, vol. 14, no. 3, p. e0213793, Mar. 2019, doi: 10.1371/JOURNAL.PONE.0213793.

[14] J. L. Kyle and E. Harris, “Global spread and persistence of dengue,” *Annu Rev Microbiol*, vol. 62, pp. 71–92, 2008, doi: 10.1146/ANNUREV.MICRO.62.081307.163005.

[15] S. A. M. Kularatne, “Dengue fever,” *BMJ*, vol. 351, Sep. 2015, doi: 10.1136/BMJ.H4661.

[16] N. Raafat, S. D. Blacksell, and R. J. Maude, “A review of dengue diagnostics and implications for surveillance and control”, doi: 10.1093/trstmh/trz068.

[17] “Dengue worldwide overview.” Accessed: Oct. 14, 2022. [Online]. Available: https://www.ecdc.europa.eu/en/dengue-monthly

[18] “Introduction to Modern Virology - Nigel J. Dimmock, Andrew J. Easton, Keith N. Leppard - Google Livros.” Accessed: Mar. 06, 2023. [Online]. Available: https://books.google.pt/books?hl=pt-PT&lr=&id=y-VbCwAAQBAJ&oi=fnd&pg=PR17&ots=01WI3cJkWe&sig=0V5_W7RA3SKRfhAcQCCevWdHKo0&redir_esc=y#v=onepage&q&f=false

[19] R. G. Huber *et al.*, “Structure mapping of dengue and Zika viruses reveals functional long-range interactions,” *Nature Communications 2019 10:1*, vol. 10, no. 1, pp. 1–13, Mar. 2019, doi: 10.1038/s41467-019-09391-8.

[20] “BioRender.” Accessed: Mar. 15, 2023. [Online]. Available: https://app.biorender.com/

[21] F. A. Rey, “Dengue virus envelope glycoprotein structure: New insight into its interactions during viral entry,” *Proc Natl Acad Sci U S A*, vol. 100, no. 12, pp. 6899–6901, Jun. 2003, doi: 10.1073/PNAS.1332695100.

[22] S. C. Harrison, “Viral membrane fusion,” *Nature Structural & Molecular Biology 2008 15:7*, vol. 15, no. 7, pp. 690–698, Jul. 2008, doi: 10.1038/nsmb.1456.

[23] O. Karimi *et al.*, “Thrombocytopenia and subcutaneous bleedings in a patient with Zika virus infection,” *The Lancet*, vol. 387, no. 10022, pp. 939–940, Mar. 2016, doi: 10.1016/S0140-6736(16)00502-X.

[24] “Fatal Zika Virus Infection with Secondary Nonsexual Transmission,” 2016, doi: 10.1056/NEJMc1610613.

[25] L. S. Muñoz, P. Barreras, and C. A. Pardo, “Zika Virus-Associated Neurological Disease in the Adult: Guillain-Barré Syndrome, Encephalitis, and Myelitis,” *Semin Reprod Med*, vol. 34, no. 5, pp. 273–279, Sep. 2016, doi: 10.1055/S-0036-1592066.

[26] R. V. da Cunha and K. S. Trinta, “Chikungunya virus: clinical aspects and treatment - A Review,” *Mem Inst Oswaldo Cruz*, vol. 112, no. 8, p. 523, 2017, doi: 10.1590/0074-02760170044.

[27] P. Renault, L. Josseran, and V. Pierre, “Chikungunya-related Fatality Rates, Mauritius, India, and Reunion Island - Volume 14, Number 8—August 2008 - Emerging Infectious Diseases journal - CDC,” *Emerg Infect Dis*, vol. 14, no. 8, p. 1327, Aug. 2008, doi: 10.3201/EID1408.080201.

[28] R. W. Ross, “The Newala epidemic: III. The virus: isolation, pathogenic properties and relationship to the epidemic,” *J Hyg (Lond)*, vol. 54, no. 2, p. 177, 1956, doi: 10.1017/S0022172400044442.

[29] H. Appassakij, P. Khuntikij, M. Kemapunmanus, R. Wutthanarungsan, and K. Silpapojakul, “Viremic profiles in asymptomatic and symptomatic chikungunya fever: a blood transfusion

threat?," *Transfusion (Paris)*, vol. 53, no. 10 Pt 2, pp. 2567–2574, 2013, doi: 10.1111/J.1537-2995.2012.03960.X.

[30] H. Y. Chong, C. Y. Leow, A. B. Abdul Majeed, and C. H. Leow, "Flavivirus infection-A review of immunopathogenesis, immunological response, and immunodiagnosis," *Virus Res*, vol. 274, Dec. 2019, doi: 10.1016/J.VIRUSRES.2019.197770.

[31] L. M. Skalinski *et al.*, "The triple epidemics of arboviruses in Feira de Santana, Brazilian Northeast: Epidemiological characteristics and diffusion patterns," *Epidemics*, vol. 38, Mar. 2022, doi: 10.1016/J.EPIDEM.2022.100541.

[32] "PAHO/WHO Data - National Dengue fever cases." Accessed: Mar. 07, 2023. [Online]. Available: https://www3.paho.org/data/index.php/en/mnu-topics/indicadores-dengue-en/dengue-nacional-en/252-dengue-pais-ano-en.html

[33] M. A. Kabir, H. Zilouchian, M. A. Younas, and W. Asghar, "Dengue Detection: Advances in Diagnostic Tools from Conventional Technology to Point of Care," *Biosensors 2021, Vol. 11, Page 206*, vol. 11, no. 7, p. 206, Jun. 2021, doi: 10.3390/BIOS11070206.

[34] L. T. Soh *et al.*, "External quality assessment of dengue and chikungunya diagnostics in the Asia Pacific region, 2015," *Western Pac Surveill Response J*, vol. 7, no. 2, p. 26, Apr. 2016, doi: 10.5365/WPSAR.2016.7.1.002.

[35] E. A. Hunsperger *et al.*, "Performance of Dengue Diagnostic Tests in a Single-Specimen Diagnostic Algorithm," *J Infect Dis*, vol. 214, no. 6, pp. 836–844, Sep. 2016, doi: 10.1093/INFDIS/JIW103.

[36] N. Houghton-Triviño, D. Montaña, and J. E. Castellanos, "Dengue-yellow fever sera cross-reactivity; challenges for diagnosis," *Rev Salud Publica (Bogota)*, vol. 10, no. 2, pp. 299–307, 2008, doi: 10.1590/S0124-00642008000200010.

[37] M. Rastogi, N. Sharma, and S. K. Singh, "Flavivirus NS1: A multifaceted enigmatic viral protein," *Virol J*, vol. 13, no. 1, pp. 1–10, Jul. 2016, doi: 10.1186/S12985-016-0590-7/FIGURES/3.

[38] V. G. da Costa, A. C. Marques-Silva, and M. L. Moreli, "A Meta-Analysis of the Diagnostic Accuracy of Two Commercial NS1 Antigen ELISA Tests for Early Dengue Virus Detection," *PLoS One*, vol. 9, no. 4, Apr. 2014, doi: 10.1371/JOURNAL.PONE.0094655.

[39] E. A. Hunsperger *et al.*, "Use of a Rapid Test for Diagnosis of Dengue during Suspected Dengue Outbreaks in Resource-Limited Regions," *J Clin Microbiol*, vol. 54, no. 8, p. 2090, Aug. 2016, doi: 10.1128/JCM.00521-16.

[40] C. V. Filomatori, M. F. Lodeiro, D. E. Alvarez, M. M. Samsa, L. Pietrasanta, and A. V. Gamarnik, "A 5′ RNA element promotes dengue virus RNA synthesis on a circular genome," *Genes Dev*, vol. 20, no. 16, p. 2238, Aug. 2006, doi: 10.1101/GAD.1444206.

[41] R. Ochsenreiter, I. L. Hofacker, and M. T. Wolfinger, "Functional RNA Structures in the 3'UTR of Tick-Borne, Insect-Specific and No-Known-Vector Flaviviruses," *bioRxiv*, p. 565580, Mar. 2019, doi: 10.1101/565580.

[42] A. Berzal-Herranz, B. Berzal-Herranz, S. E. Ramos-Lorente, and C. Romero-López, "The Genomic 3′ UTR of Flaviviruses Is a Translation Initiation Enhancer," *Int J Mol Sci*, vol. 23, no. 15, Aug. 2022, doi: 10.3390/IJMS23158604.

[43] L. de Borba *et al.*, “RNA Structure Duplication in the Dengue Virus 3’ UTR: Redundancy or Host Specificity?,” *mBio*, vol. 10, no. 1, Jan. 2019, doi: 10.1128/MBIO.02506-18.

[44] B. B. Oliveira, B. Veigas, and P. V. Baptista, “Isothermal Amplification of Nucleic Acids: The Race for the Next ‘Gold Standard,’” *Frontiers in Sensors*, vol. 2, Sep. 2021, doi: 10.3389/FSENS.2021.752600.

[45] L. Garibyan and N. Avashia, “Research Techniques Made Simple: Polymerase Chain Reaction (PCR),” *J Invest Dermatol*, vol. 133, no. 3, p. e6, 2013, doi: 10.1038/JID.2013.1.

[46] Mónica Sebastiana, “PCR-Polymerase Chain Reaction & Agarose Gel Electrophoresis,” *Fisiologia Molecular do Stress*. Ciências ULisboa, Biologia vegetal.

[47] Primer Design, “Beginner’s Guide to Real-Time PCR.” Accessed: Mar. 14, 2023. [Online]. Available: http://www.primerdesign.co.uk/assets/files/beginners_guide_to_real_time_pcr.pdf

[48] Y. Mardian, H. Kosasih, M. Karyana, A. Neal, and C. Y. Lau, “Review of Current COVID-19 Diagnostics and Opportunities for Further Development,” *Front Med (Lausanne)*, vol. 8, p. 562, May 2021, doi: 10.3389/FMED.2021.615099/BIBTEX.

[49] Thermo Fisher Scientific, “PCR Setup—Six Critical Components to Consider.” Accessed: Aug. 18, 2023. [Online]. Available: https://www.thermofisher.com/ch/en/home/life-science/cloning/cloning-learning-center/invitrogen-school-of-molecular-biology/pcr-education/pcr-reagents-enzymes/pcr-component-considerations.html

[50] H. D. VanGuilder, K. E. Vrana, and W. M. Freeman, “Twenty-five years of quantitative PCR for gene expression analysis,” *Biotechniques*, vol. 44, no. 5, pp. 619–626, Apr. 2008, doi: 10.2144/000112776.

[51] “All about Probe-Based Real-Time qPCR Assays | GoldBio.” Accessed: Aug. 13, 2023. [Online]. Available: https://goldbio.com/articles/article/all-about-probe-based-qPCR

[52] “BHQplus Probes | LGC Biosearch Technologies.” Accessed: Aug. 13, 2023. [Online]. Available: https://www.biosearchtech.com/products/pcr-reagents-kits-and-instruments/pcr-probes-and-assays/custom-dna-probes-for-qpcr/bhqplus-probes

[53] M. A. Valasek and J. J. Repa, “The power of real-time PCR,” *Adv Physiol Educ*, vol. 29, no. 3, pp. 151–159, 2005, doi: 10.1152/ADVAN.00019.2005.

[54] C. J. Smith and A. M. Osborn, “Advantages and limitations of quantitative PCR (Q-PCR)-based approaches in microbial ecology,” *FEMS Microbiol Ecol*, vol. 67, no. 1, pp. 6–20, Jan. 2009, doi: 10.1111/J.1574-6941.2008.00629.X.

[55] “Veriti™ 96-Well Fast Thermal Cycler.” Accessed: Oct. 14, 2023. [Online]. Available: https://www.thermofisher.com/order/catalog/product/4375305?SID=srch-srp-4375305

[56] F. Najioullah, F. Viron, and R. Césaire, “Evaluation of four commercial real-time RT-PCR kits for the detection of dengue viruses in clinical samples,” *Virol J*, vol. 11, no. 1, Sep. 2014, doi: 10.1186/1743-422X-11-164.

[57] Wisconsin Veterinary Diagnostic Laboratory University of Wisconsin–Madison, “Real Time PCR Ct Values.” Accessed: Sep. 26, 2023. [Online]. Available: https://www.wvdl.wisc.edu/wp-content/uploads/2013/01/WVDL.Info_.PCR_Ct_Values1.pdf

[58] “Understanding qPCR Efficiency and Why It Exceeds 100%.” Accessed: Sep. 26, 2023. [Online]. Available: https://biosistemika.com/blog/qpcr-efficiency-over-100/

[59] S. Kumar, “Isothermal Nucleic Acid Amplification System: An Update on Methods and Applications,” 2018.

[60] X. Fan *et al.*, “Clinical Validation of Two Recombinase-Based Isothermal Amplification Assays (RPA/RAA) for the Rapid Detection of African Swine Fever Virus,” *Front Microbiol*, vol. 11, p. 1696, Jul. 2020, doi: 10.3389/FMICB.2020.01696/BIBTEX.

[61] T. Jiang *et al.*, “Recombinase Polymerase Amplification Combined with Real-Time Fluorescent Probe for Mycoplasma pneumoniae Detection,” *Journal of Clinical Medicine 2022, Vol. 11, Page 1780*, vol. 11, no. 7, p. 1780, Mar. 2022, doi: 10.3390/JCM11071780.

[62] O. Piepenburg, C. H. Williams, D. L. Stemple, and N. A. Armes, “DNA Detection Using Recombination Proteins,” *PLoS Biol*, vol. 4, no. 7, pp. 1115–1121, 2006, doi: 10.1371/JOURNAL.PBIO.0040204.

[63] A. S. James and J. I. Alwneh, “COVID-19 infection diagnosis: Potential impact of isothermal amplification technology to reduce community transmission of SARS-CoV-2,” *Diagnostics*, vol. 10, no. 6, Jun. 2020, doi: 10.3390/DIAGNOSTICS10060399.

[64] R. K. Daher, G. Stewart, M. Boissinot, and M. G. Bergeron, “Recombinase Polymerase Amplification for Diagnostic Applications,” *Clin Chem*, vol. 62, no. 7, p. 947, Jul. 2016, doi: 10.1373/CLINCHEM.2015.245829.

[65] R. K. Daher, G. Stewart, M. Boissinot, and M. G. Bergeron, “Recombinase polymerase amplification for diagnostic applications,” *Clin Chem*, vol. 62, no. 7, pp. 947–958, Jul. 2016, doi: 10.1373/CLINCHEM.2015.245829.

[66] “Recombinase Polymerase Amplification & Lateral Flow.” Accessed: Mar. 10, 2023. [Online]. Available: https://www.milenia-biotec.com/en/method/recombinase-polymerase-amplification/

[67] R. Y. Alhabbab *et al.*, “Amplifying Lateral Flow Assay Signals for Rapid Detection of COVID-19 Specific Antibodies,” *Global Challenges*, vol. 6, no. 7, p. 2200008, Jul. 2022, doi: 10.1002/GCH2.202200008.

[68] M. L. Boisen *et al.*, “Development of Prototype Filovirus Recombinant Antigen Immunoassays,” 2015, doi: 10.1093/infdis/jiv353.

[69] H. N. Lee, J. Lee, Y. K. Kang, J. H. Lee, S. Yang, and H. J. Chung, “A Lateral Flow Assay for Nucleic Acid Detection Based on Rolling Circle Amplification Using Capture Ligand-Modified Oligonucleotides,” *Biochip J*, vol. 16, no. 4, pp. 441–450, Dec. 2022, doi: 10.1007/S13206-022-00080-1/FIGURES/6.

[70] K. M. Koczula and A. Gallotta, “Lateral flow assays,” *Essays Biochem*, vol. 60, no. 1, p. 111, Jun. 2016, doi: 10.1042/EBC20150012.

[71] A. C. Mirica, D. Stan, I. C. Chelcea, C. M. Mihailescu, A. Ofiteru, and L. A. Bocancia-Mateescu, “Latest Trends in Lateral Flow Immunoassay (LFIA) Detection Labels and Conjugation Process,” *Front Bioeng Biotechnol*, vol. 10, p. 984, Jun. 2022, doi: 10.3389/FBIOE.2022.922772/BIBTEX.

[72] B. Zhang, Z. Zhu, F. Li, X. Xie, and A. Ding, “Rapid and sensitive detection of hepatitis B virus by lateral flow recombinase polymerase amplification assay,” *J Virol Methods*, vol. 291, p. 114094, May 2021, doi: 10.1016/J.JVIROMET.2021.114094.

[73] Z. ran Li *et al.*, “Development and evaluation of recombinase polymerase amplification combined with lateral flow dipstick assays for co-detection of epizootic haemorrhagic disease virus and the Palyam serogroup virus,” *BMC Vet Res*, vol. 17, no. 1, pp. 1–11, Dec. 2021, doi: 10.1186/S12917-021-02977-9/TABLES/2.

[74] Y. zhong Xu, D. zhi Fang, F. fang Chen, Q. fei Zhao, C. ming Cai, and M. gang Cheng, “Utilization of recombinase polymerase amplification method combined with lateral flow dipstick for visual detection of respiratory syncytial virus,” *Mol Cell Probes*, vol. 49, Feb. 2020, doi: 10.1016/J.MCP.2019.101473.

[75] A. V. Ivanov, I. V. Safenkova, A. V. Zherdev, and B. B. Dzantiev, “Recombinase polymerase amplification assay with and without nuclease-dependent-labeled oligonucleotide probe,” *Int J Mol Sci*, vol. 22, no. 21, p. 11885, Nov. 2021, doi: 10.3390/IJMS222111885/S1.

[76] R. Franco, P. Pedrosa, F. F. Carlos, B. Veigas, and P. V. Baptista, “Gold Nanoparticles for DNA/RNA-Based Diagnostics,” *Handbook of Nanoparticles*, p. 1339, Sep. 2015, doi: 10.1007/978-3-319-15338-4_31.

[77] H. Li, Y. Zhang, L. Wang, J. Tian, and X. Sun, “Nucleic acid detection using carbon nanoparticles as a fluorescent sensing platform,” *Chemical Communications*, vol. 47, no. 3, pp. 961–963, Dec. 2010, doi: 10.1039/C0CC04326E.

[78] Savile. Bradbury and Peter. Evennett, *Contrast techniques in light microscopy*. Bios Scientific Publishers, 1996. Accessed: Jun. 29, 2023. [Online]. Available: https://www.routledge.com/Contrast-Techniques-in-Light-Microscopy/Evennett/p/book/9781859960851

[79] “Capillary blood - Can it replace venous blood?” Accessed: Oct. 15, 2023. [Online]. Available: https://www.human.de/lab-professionals/trends-topics/capillary-blood-can-it-replace-venous-blood

[80] “SD BIOLINE Dengue Duo | NS1 Ag & IgG/IgM test | 11FK46 | ABBOTT | Standard Diagnostics, Inc.” Accessed: Oct. 15, 2023. [Online]. Available: https://maxanim.com/rapid-tests/sd-bioline-dengue-duo/

[81] R. P. Wilkes *et al.*, “Rapid and sensitive insulated isothermal PCR for point-of-need feline leukaemia virus detection,” *J Feline Med Surg*, vol. 20, no. 4, pp. 362–369, Apr. 2018, doi: 10.1177/1098612X17712847.

[82] L. D. Piedrahita, I. Y. Agudelo, A. I. Trujillo, R. E. Ramírez, J. E. Osorio, and B. N. Restrepo, “Evaluation of Commercially Available Assays for Diagnosis of Acute Dengue in Schoolchildren during an Epidemic Period in Medellin, Colombia,” *Am J Trop Med Hyg*, vol. 95, no. 2, p. 315, Aug. 2016, doi: 10.4269/AJTMH.15-0492.

[83] A. M. Anand, S. Sistla, R. Dhodapkar, A. Hamide, N. Biswal, and B. Srinivasan, “Evaluation of NS1 Antigen Detection for Early Diagnosis of Dengue in a Tertiary Hospital in Southern India,” *J Clin Diagn Res*, vol. 10, no. 4, p. DC01, Apr. 2016, doi: 10.7860/JCDR/2016/15758.7562.

[84] Y. Y. Go *et al.*, "A Pan-Dengue Virus Reverse Transcription-Insulated Isothermal PCR Assay Intended for Point-of-Need Diagnosis of Dengue Virus Infection by Use of the POCKIT Nucleic Acid Analyzer," *J Clin Microbiol*, vol. 54, no. 6, pp. 1528–1535, Jun. 2016, doi: 10.1128/JCM.00225-16.

[85] M. Neeraja *et al.*, "Rapid detection and differentiation of dengue virus serotypes by NS1 specific reverse transcription loop-mediated isothermal amplification (RT-LAMP) assay in patients presenting to a tertiary care hospital in Hyderabad, India," *J Virol Methods*, vol. 211, p. 22, Jan. 2015, doi: 10.1016/J.JVIROMET.2014.10.005.

[86] J. J. L. Tan *et al.*, "An Integrated Lab-on-Chip for Rapid Identification and Simultaneous Differentiation of Tropical Pathogens," *PLoS Negl Trop Dis*, vol. 8, no. 7, p. 3043, 2014, doi: 10.1371/JOURNAL.PNTD.0003043.

[87] G. Añez, D. A. Heisey, E. Volkova, and M. Rios, "Complete Genome Sequences of Dengue Virus Type 1 to 4 Strains Used for the Development of CBER/FDA RNA Reference Reagents and WHO International Standard Candidates for Nucleic Acid Testing," *Genome Announc*, vol. 4, no. 1, 2016, doi: 10.1128/GENOMEA.01583-15.

[88] O. J. Marshall, "PerlPrimer: cross-platform, graphical primer design for standard, bisulphite and real-time PCR," *Bioinformatics*, vol. 20, no. 15, pp. 2471–2472, Oct. 2004, doi: 10.1093/BIOINFORMATICS/BTH254.

[89] B. T. Teoh *et al.*, "Early Detection of Dengue Virus by Use of Reverse Transcription-Recombinase Polymerase Amplification," *J Clin Microbiol*, vol. 53, no. 3, p. 830, Mar. 2015, doi: 10.1128/JCM.02648-14.

[90] E. Alm *et al.*, "Universal Single-Probe RT-PCR Assay for Diagnosis of Dengue Virus Infections," *PLoS Negl Trop Dis*, vol. 8, no. 12, Dec. 2014, doi: 10.1371/JOURNAL.PNTD.0003416.

[91] Y. Xi, C. Z. Xu, Z. Z. Xie, D. L. Zhu, and J. M. Dong, "Rapid and visual detection of dengue virus using recombinase polymerase amplification method combined with lateral flow dipstick," *Mol Cell Probes*, vol. 46, Aug. 2019, doi: 10.1016/J.MCP.2019.06.003.

[92] "Spectrum [FAM (Carboxyfluorescein)] | AAT Bioquest." Accessed: Oct. 15, 2023. [Online]. Available: https://www.aatbio.com/fluorescence-excitation-emission-spectrum-graph-viewer/fam_carboxyfluorescein

[93] M. M. Kaminski *et al.*, "A CRISPR-based assay for the detection of opportunistic infections post-transplantation and for the monitoring of transplant rejection," *Nature Biomedical Engineering 2020 4:6*, vol. 4, no. 6, pp. 601–609, Apr. 2020, doi: 10.1038/s41551-020-0546-5.

[94] M. Burns and H. Valdivia, "Modelling the limit of detection in real-time quantitative PCR," *European Food Research and Technology*, vol. 226, no. 6, pp. 1513–1524, Apr. 2008, doi: 10.1007/S00217-007-0683-Z/METRICS.

[95] "spinit® - biosurfit." Accessed: Aug. 21, 2023. [Online]. Available: https://www.biosurfit.com/en/spinit/

[96] "Understanding qPCR Efficiency and Why It Exceeds 100%." Accessed: Sep. 06, 2023. [Online]. Available: https://biosistemika.com/blog/qpcr-efficiency-over-100/

[97] "Choosing the right agarose percentage for gel electrophoresis – miniPCR bio." Accessed: Aug. 19, 2023. [Online]. Available: https://www.minipcr.com/choosing-the-right-agarose-percentage/

[98] "TwistAmp ™ Liquid exo Quick Guide Part number: INLQEXO Revision 3," 2019, Accessed: Aug. 22, 2023. [Online]. Available: https://www.twistdx.co.uk/terms-of-supply,

[99] S. A. Ejazi *et al.*, "Development and clinical evaluation of serum and urine-based lateral flow tests for diagnosis of human visceral leishmaniasis," *Microorganisms*, vol. 9, no. 7, Jul. 2021, doi: 10.3390/MICROORGANISMS9071369.

[100] A. N. Danthanarayana *et al.*, "Smartphone-readable RPA-LFA for the high-sensitivity detection of Leishmania kDNA using nanophosphor reporters," *PLoS Negl Trop Dis*, vol. 17, no. 7, p. e0011436, Jul. 2023, doi: 10.1371/JOURNAL.PNTD.0011436.

[101] A. Abd El Wahed *et al.*, "Recombinase Polymerase Amplification Assay for Rapid Diagnostics of Dengue Infection," *PLoS One*, vol. 10, no. 6, Jun. 2015, doi: 10.1371/JOURNAL.PONE.0129682.

[102] W. K. Wang, T. L. Sung, Y. C. Tsai, C. L. Kao, S. M. Chang, and C. C. King, "Detection of Dengue Virus Replication in Peripheral Blood Mononuclear Cells from Dengue Virus Type 2-Infected Patients by a Reverse Transcription-Real-Time PCR Assay," *J Clin Microbiol*, vol. 40, no. 12, p. 4472, Dec. 2002, doi: 10.1128/JCM.40.12.4472-4478.2002.

[103] Y. Wang *et al.*, "Establishment and Clinical Application of a RPA-LFS Assay for Detection of Capsulated and Non-Capsulated Haemophilus influenzae," *Front Cell Infect Microbiol*, vol. 12, Apr. 2022, doi: 10.3389/FCIMB.2022.878813.

# 6. SUPPLEMENTARY MATERIAL

aaggcaaa actaacatga aacaaggcta gaagtcaggt cggattaagc catagtacgg aaaaaactat gctacctgtg agccccgtcc aaggacgtta aaagaagtca ggccattaca aatgccatag cttgagtaaa ctgtgcagcc tgtagctcca cctgagaagg tgtaaaaaat ctgggaggcc acaaaccatg gaagctgtac gcatggcgta gtggactagc ggttagagga gacccctccc ttacaaatcg cagcaacaat gggggcccaa ggtgagatga agctgtagtc tcactggaag gactagaggt tagaggagac ccccccaaaa caaaaaacag catattgacg ctgggaaaga ccagagatcc tgctgtctcc tcagcatcat tccaggcaca gaacgccaga aaatggaatg gtgctgttga atcaacaggt tct

**Figure 44: Sequence of the 3'UTR gene of DENV NGC (KM204118)(10273-10723).**

**Figure 45: LFA strip interfering with the bonding of the closing tape.**

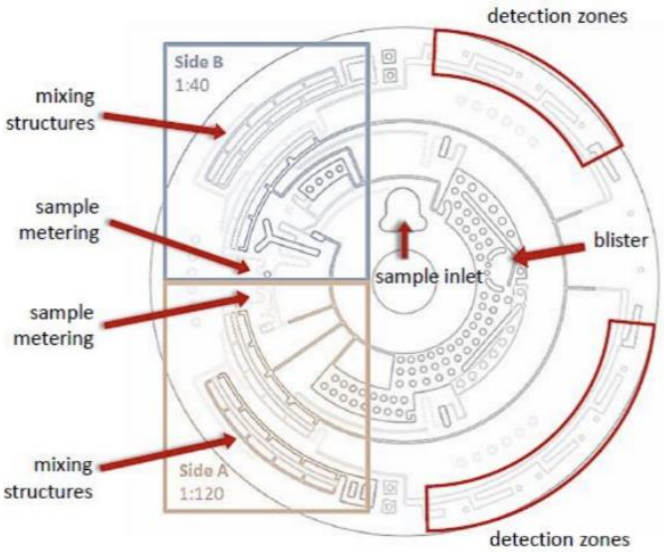


**Figure 46: Layout of the CRP disc with identification of the microfluidic structures.**

## PCR1.2 assay

This assay was done by the co-supervisor of this thesis Dr. Catarina Caneira at the laboratory of analysis from the Instituto Superior Tecnico da Universidade de Lisboa. It is a conventional PCR with detection by agarose gel electrophoresis. The master mix contains 0.8 µM of each primer and no probe was used for this assay. The thermal cycle's parameters were the following: an initial denaturation at 94°C for 10 min, 40 cycles of a 3-step amplification with 1 min at 94°C, 1 min at the annealing temperature and 1 min at 72°C. Then a final extension at 72°C for 15 min. Two different annealing temperatures were tested for this assay: 56°C and 58°C. For each temperature, the assay contains a blank, two replicas with $10^4$ copies/mL of target, two replicas with $10^5$ copies/mL of target, one control with nuclease-free water replacing the primers, probe and target and one control with water replacing the primer and probe, with a target of $10^5$ copies/mL.

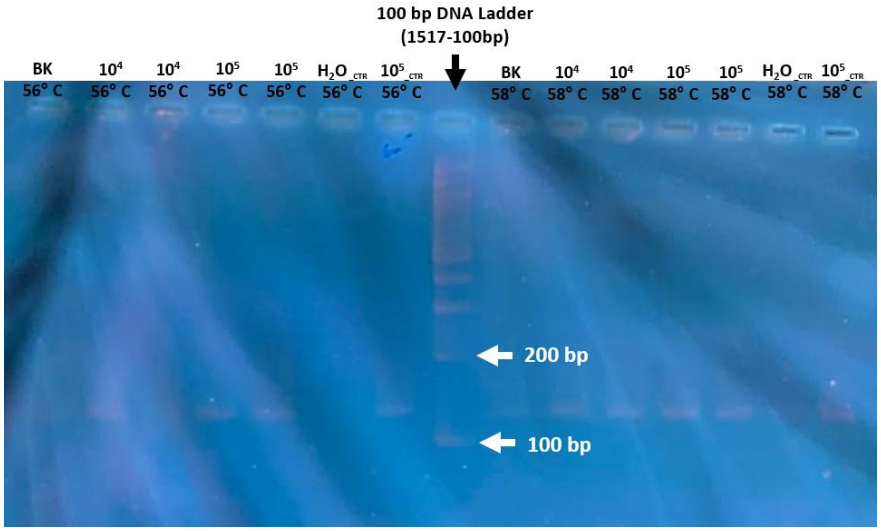


**Figure 47: Agarose gel electrophoresis of PCR1.2. CTR is positive control with the same reagents used for the previous assay PCR1.1.**

This assay showed a product in almost all the samples except the ones containing only water, with an expected product of amplification of 128 bp. This shows could have been the result of a contamination of the reagents but this assay was done in a different laboratory than the usual one, with a different person from the previous assays and with new reagents that were freshly opened (except for the positive control). This eliminates the hypothesis of contamination and leads towards the fact that this is probably the result of the formation of primer dimers that coincidentally have a similar size to the expected amplicon.

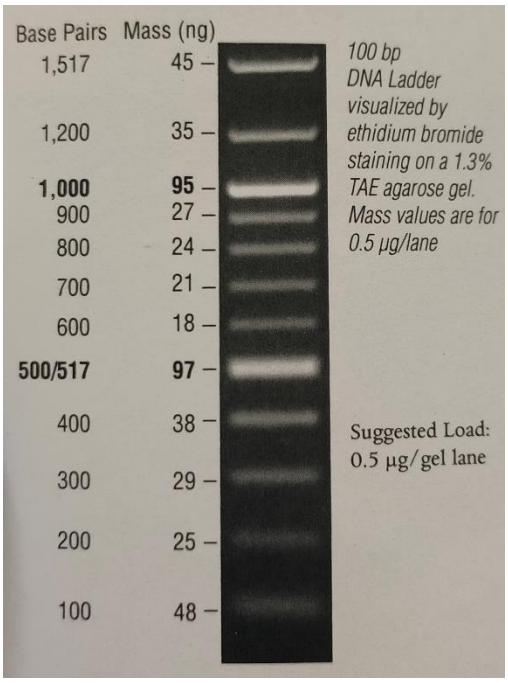


**Figure 48: 100 bp DNA Ladder N3231S (New England BioLabs, USA).**

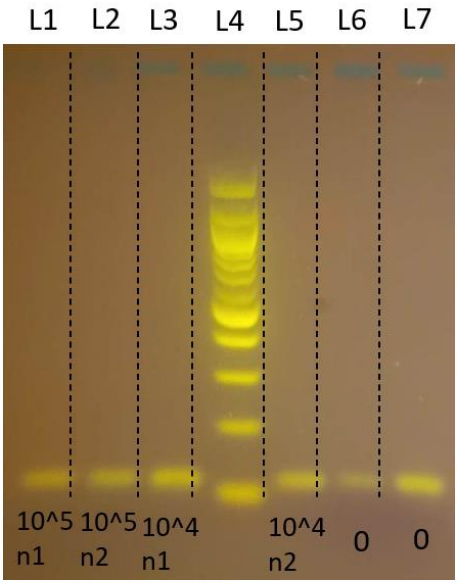


**Figure 49: Agarose gel electrophoresis of PCR2 (2.5% agarose).**